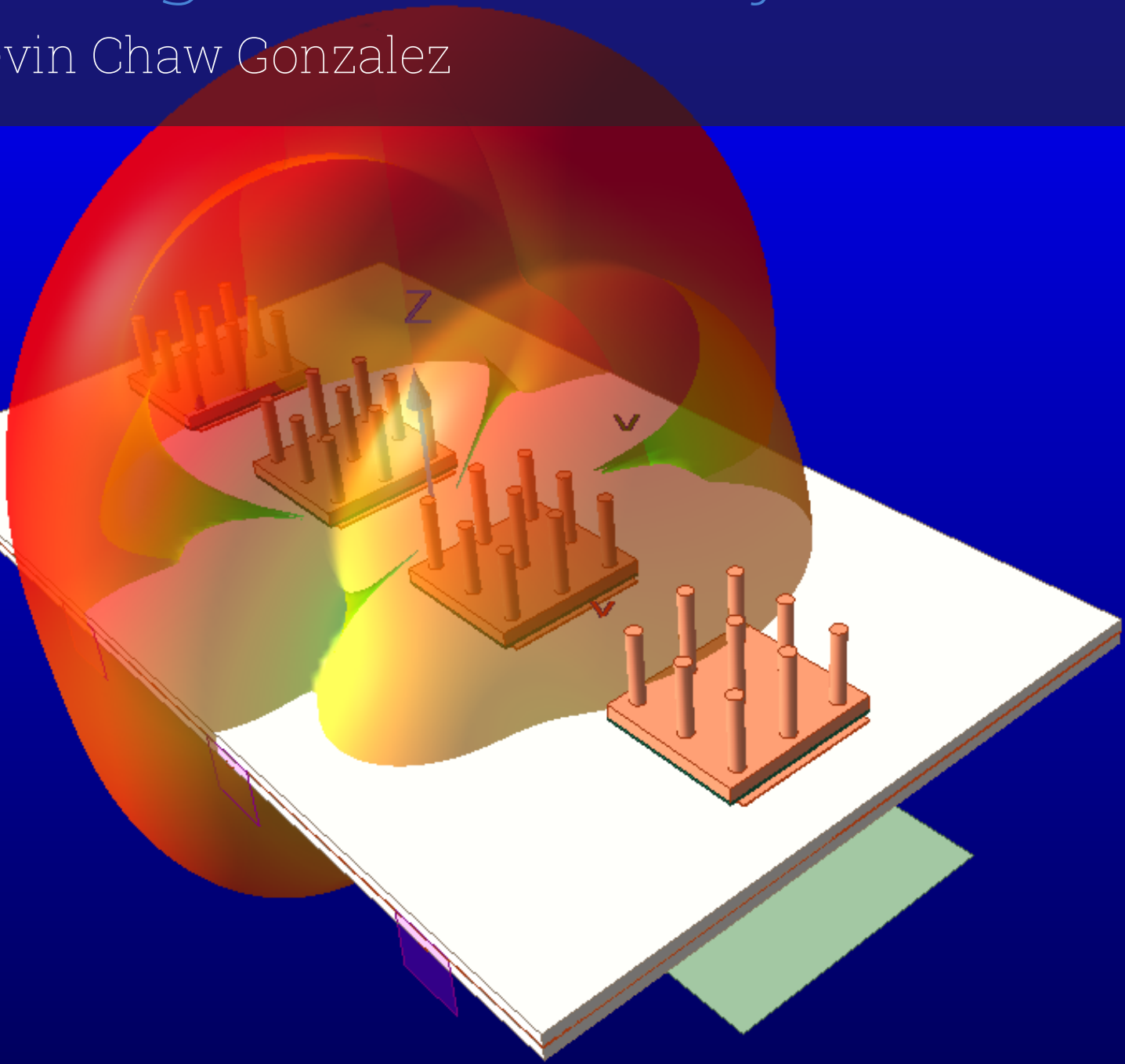


# Differential Aperture Fed Heatsink Antenna Design and Analysis

Kevin Chaw Gonzalez

Delft University of Technology



# Differential Aperture Fed Heatsink Antenna Design and Analysis

by

Kevin Chaw Gonzalez

To obtain the degree of Master of Science in Electrical Engineering at the Delft University of Technology, to be defended publicly on December 12, 2024 at 9:00.

Supervisor: A. Yarovoy  
Daily supervisor: Y. Aslan  
External Supervisor: M. Spirito  
Student number: 5351057  
Project Duration: June, 2024 - December, 2024  
Faculty: Faculty of Electrical Engineering, Mathematics and Computer Science, Delft

# Acknowledgment

This thesis represents the culmination of collaborative efforts and steadfast support that have inspired and sustained my academic journey. The process of exploration and learning has been profoundly rewarding, presenting countless opportunities for growth and self-discovery. It is no exaggeration to say that this experience has been one of the most transformative periods of my life. I am deeply indebted to my supervisors and peers, whose expertise, guidance, and encouragement have been instrumental in shaping the direction and success of this work.

I extend my sincere gratitude to Prof. DSc Alexander Yarovoy for granting me the opportunity to work with the Microwave Sensing, Signals, and Systems (MS3) group during my thesis. Your unwavering support and insightful mentorship have set a high standard for the professional excellence I aim to achieve. The research group you have so diligently cultivated is a testament to your vision and leadership.

The exceptional talent, collaborative spirit, and culture of innovation within the MS3 group have been a constant source of inspiration and support throughout my master's program. The dedication and brilliance of the students, PhD candidates, and professors make this group an extraordinary environment for learning and growth. Working alongside such remarkable individuals has enriched my academic journey and profoundly shaped my perspective on research and problem-solving.

I owe immense gratitude to my supervisor, Dr. Yanki Aslan. Your patience, dedication, and unwavering support have been pivotal to the completion of this work. Your kindness and empathy during my most challenging moments gave me the strength to persevere. Your clear and thoughtful guidance has been instrumental in every step of this journey.

I also extend my utmost thanks to Feza Celik, whose generosity with his time and remarkable understanding of complex topics helped me address critical gaps in my knowledge. Your willingness to assist and share your expertise has been invaluable.

To my brother and sister, thank you for always having my back and supporting me unconditionally throughout this time. Your encouragement has meant more to me than words can express.

Lastly, I am profoundly grateful to my parents. Not only have you paved the way for me with your sacrifices and unwavering support, but you have also stood by me at every step of this journey. Even in moments of disagreement, your love has never faltered, and for that, I am forever grateful.

*Kevin Chaw Gonzalez  
Delft, December 2024*

# Abstract

As 5G mm-wave communication progresses toward higher frequencies to meet market demands, companies are being pushed to adopt cutting-edge technologies. Operating at these higher frequencies naturally leads to shorter wavelengths, which increases circuit density. This higher density, in turn, complicates heat management. A supplementary solution involving heatsink antennas has been proposed to address this issue.

Recent research from the MS3 group introduces a cost-effective, dual-functional pin-fed shorted patch antenna designed to assist with heat dissipation. Although the integration of a heatsink significantly improves thermal management, it does so at the cost of electromagnetic (EM) performance, particularly affecting radiation pattern symmetry, cross-polarization levels, and bandwidth. This work builds upon the latest research by using the aforementioned design as a benchmark, exploring further improvements and addressing the challenges introduced by the heatsink.

This work presents, for the first time, the use of differential feeding to address the performance degradation caused by the heatsink. Differential feeding has been shown to enhance radiation pattern symmetry, increase gain, and improve bandwidth in certain applications. Additionally, aperture coupling is employed to further enhance the impedance bandwidth of the shorted patch. The results at the element level indicate a 90% improvement in impedance bandwidth due to aperture coupling; however, this comes with a significant degradation in the radiation pattern.

By integrating aperture-coupled differential feeding, this work demonstrates symmetric radiation patterns, an improved bandwidth compared to the benchmark, and reduced cross-polarization levels. At the array level, differential feeding leads to a higher degree of coupling than pin-fed patch arrays for spacing values less than or equal to  $0.6\lambda$ . Furthermore, differential feeding improves gain, reduces cross-polarization levels, and enhances radiation pattern symmetry compared to the benchmark.

# Contents

<b>Acknowledgment</b>	<b>i</b>
<b>Abstract</b>	<b>ii</b>
<b>Nomenclature</b>	<b>viii</b>
<b>1 Introduction</b>	<b>1</b>
1.1 Motivation . . . . .	1
1.2 Latest research at MS3 on heatsink antennas . . . . .	3
1.3 Problem Formulation . . . . .	4
1.4 Objectives . . . . .	5
1.5 Scope . . . . .	5
1.6 Novelties . . . . .	6
1.7 Thesis structure . . . . .	6
<b>2 Theoretical Background and Literature Review</b>	<b>7</b>
2.1 Theoretical Background . . . . .	7
2.1.1 Aperture coupled patch antenna feeding in patch antennas . . . . .	7
2.2 Literature Review . . . . .	10
2.2.1 Heatsink Antennas . . . . .	10
2.2.2 Differentially fed patch . . . . .	13
2.3 Conclusions . . . . .	16
2.3.1 On heatsinks . . . . .	16
2.3.2 On differential feeding . . . . .	17
<b>3 Heatsink Antenna Element</b>	<b>18</b>
3.1 The benchmark- Pin fed heatsink antenna model . . . . .	18
3.2 Aperture coupled patch model with and without heatsink . . . . .	19
3.3 Differential aperture coupled patch . . . . .	20
3.3.1 Power divider design . . . . .	20
3.3.2 Differentially fed patch element . . . . .	21
3.4 Single elements results . . . . .	22
3.4.1 Aperture Coupling Performance and the Impact of Heatsink Integration . . . . .	22
3.4.2 Differential Feeding Integration Results . . . . .	25
<b>4 Differential Array Design</b>	<b>27</b>
4.1 Linear array differential differential and pin feed considerations . . . . .	27
4.2 Linear array results . . . . .	27
4.2.1 Impedance and Coupling Performance . . . . .	27
4.2.2 Radiation Pattern Characteristics . . . . .	28
4.2.3 Phase Shift and Beam Steering . . . . .	28

- 5 Conclusion** **34**
- 5.1 Conclusion . . . . . 34
- 5.2 Recommendations . . . . . 35
- References** **36**
- A Appendix A** **39**
- B Appendix B** **41**

# List of Figures

1.1	Examples of heat management structures . . . . .	2
1.2	Comparison of IC power density in silicon based scaled phased array[11]	3
1.3	Pin-fed shorted patch design . . . . .	4
1.4	Fin heatsink antennas models proposed by the MS3 group[12] . . . . .	4
1.5	Heatsink antennas $S_{11}$ . . . . .	5
2.1	Aperture coupled patch parameters . . . . .	7
2.2	Slot shapes . . . . .	8
2.3	Effects of aperture width, stub length and aperture separation on coupling and bandwidth of a patch antenna represented on smith chart . . . . .	9
2.4	Antennas with heatsinks . . . . .	10
2.5	Heatsink as antennas . . . . .	11
2.6	Aperture antennas with heatsink and fractal heatsink . . . . .	12
2.7	Differential patch antennas . . . . .	13
2.8	Differential dual polarized aperture coupled . . . . .	15
2.9	Differential aperture coupled feeding scheme . . . . .	15
2.10	[35](a)Antenna element (b)Equivalent circuit (c) Filtering capabilities . .	16
2.11	Differential patch antennas . . . . .	17
3.1	Pin fed patch with heatsink [benchmark] . . . . .	18
3.2	Single aperture coupled patches with heatsink (a), and without heatsink (b) . . . . .	19
3.3	PSPD performance . . . . .	20
3.4	Differential heatsink antenna and PSPD . . . . .	21
3.5	$S_{11}$ comparison between single aperture without heatsink, single aperture with heatsink and Pin fed with heatsink. . . . .	22
3.6	Aperture coupled patch with heatsink . . . . .	23
3.7	Pin fed patch patch with heatsink . . . . .	24
3.8	Radiation bandwidth comparison between Differential patch (a) and Single Pin fed Patch (b). . . . .	25
3.9	Differentially fed patch with heatsink . . . . .	26
4.1	Four element shorted patch linear arrays (a) Differentially fed and (b) single pin fed with heatsinks, for phased array analysis. . . . .	28
4.2	Four element pin fed array Active S-parameter at several spacings between elements. Progressive phase shift = 0. . . . .	29
4.3	Four element differential array Active S-parameter at several spacings between elements. Progressive phase shift = 0. . . . .	30
4.4	Four element Differential array co-polarized realized gain results. $0^\circ, 60^\circ, 90^\circ, 120^\circ$ phase shifts are applied for several spacings between elements. . . . .	31

- 4.5 Four element Pin fed array co-polarized realized gain results.  $0^\circ, 60^\circ, 90^\circ, 120^\circ$  phase shifts are applied for several spacings between elements. . . . . 32
- 4.6 Realized gain and Active S parameter comparison of Pin fed and Differentially fed linear arrays. Gains are plotted for 28 GHz . . . . . 33
  
- B.1 Four element pin fed array with heatsink active S parameters with a progressive phase shift of:  $30^\circ, 60^\circ, 90^\circ, 120^\circ$  . . . . . 41
- B.2 Four element differentially fed array with heatsink active S parameters with a progressive phase shift of:  $30^\circ, 60^\circ, 90^\circ, 120^\circ$  . . . . . 42

# List of Tables

1.1	Chip temperature per heatsink antenna topology . . . . .	4
4.1	Table comparing differential and pin fed linear array co-pol, x-pol, and sidelobe levels for $0.5\lambda$ spacing between elements. . . . .	29
A.1	Phase and amplitude tapering for a two port shorted differentially fed patch antenna. Port imbalance is symmetrical and interchangeable. . . .	40

# Nomenclature

<b>SoC</b>	System-on-Chip
<b>EMI</b>	Electromagnetic Interference
<b>AiP</b>	Antenna-in-Package
<b>PA</b>	Power Amplifier
<b>PCB</b>	Printed Circuit Board
<b>SIW</b>	Substrate integrated waveguide
<b>AESA</b>	Active electronically steered array
<b>DPA</b>	Differential patch antenna
<b>MS3</b>	Microwave Sensing, Signal and Systems
<b>PSPD</b>	Phase shifted power divider

# 1

## Introduction

### 1.1. Motivation

Over the past four decades, there has been a significant focus on improving the efficiency and reliability of communication technologies. With growing market demands for faster data rates, lower latency, and wider transmission bandwidths, companies have been driven to innovate and develop cutting-edge solutions. One of the most transformative responses to these demands has been the introduction of 5G communication technology, which capitalizes on the mm-wave spectrum to achieve improved performance [1].

A key advancement within 5G is the development of Active Electronically Scanned Arrays (AESA), which now support fully digital beamforming. This allows for the creation of multiple simultaneous beams, a breakthrough that enhances mobile communication systems through Beam-Division Multiple Access, significantly improving network capacity and user experiences.[2]

However, while these advancements bring immense potential, they also introduce new challenges. Ensuring that these systems remain reliable and robust under the increased complexity of 5G technology will require addressing issues such as heat dissipation, power efficiency, and signal interference, all of which are critical to sustaining long-term performance.

A major challenge faced by 5G technology is the limitation of excess heat dissipation. Excessive heat can rapidly degrade the lifetime and reliability of electronic devices, with high circuit temperatures accounting for up to 55% of system failures, as noted by Abdullah et al. [3]. Additionally, heat affects the data rates users experience through their carrier services. For example, sustained downloading of high-bandwidth streams for 15 minutes can significantly increase the temperature of a 5G base station [4]. To maintain continuous cellphone service, carriers may need to downgrade their 5G services to 4G/LTE under these conditions.

Several factors contribute to excess heat generation. One of the primary sources is the inefficiency of silicon-based power amplifiers (PAs), which typically achieve only around 30% efficiency [2]. Additionally, the compact nature of printed circuit boards (PCBs) and system packages, driven by the shorter wavelengths of the mm-wave frequency band,

necessitates smaller circuit dimensions. This results in higher power density ( $\text{W}/\text{cm}^2$ ), presenting a critical challenge to PCB reliability. The integration of active electronically scanned arrays (AESAs) further complicates system design, as each antenna element in the array requires its own chip. [2] While higher integration is desirable, particularly for mobile devices, managing power density becomes a key concern. Figure 1.2 highlights the relationship between power density and higher operating frequencies.

A few conventional solutions are used in heat dissipation. Among them, heatsinks remain one of the most widely used solutions in the industry for heat management. Considerable research has been devoted to improving the efficiency of heat dissipation from heatsinks, focusing on the topology of the heatsink as well as material composition [3] [5]. Other methods include active fan cooling, fractal heatsinks, microfluidic channels, and even unconventional techniques such as a flapping wing design [6] [7] [8]. Despite these advancements, these methods have proven insufficient to the increasingly complex thermal management of the base stations.

An approach that has caught some attention recently is the integration of heatsink antennas or antenna elements [9]. The heatsink antennas can introduce and build up on the current heat management options for AiP solutions. The concept consists of directly attaching a heatsink to an antenna to draw out as much heat from the chips as possible. Attaching a heatsink not only improves heat dissipation but also improves certain aspects of radiation and matching in an antenna. However, it also introduces some trade offs and considerations such as impedance and radiation bandwidth, pattern asymmetry, cross-polarization levels, will be discussed in further sections.

This work will build upon the latest research and advancements conducted at TU Delft. Within the Microwave Sensing, Signal and Systems (MS3) group, innovative approaches and new considerations for heatsink integration are being explored. This project aims to enhance and expand upon the most recent and relevant developments by the group in the field of heatsink antennas.



**Figure 1.1:** Examples of heat management structures

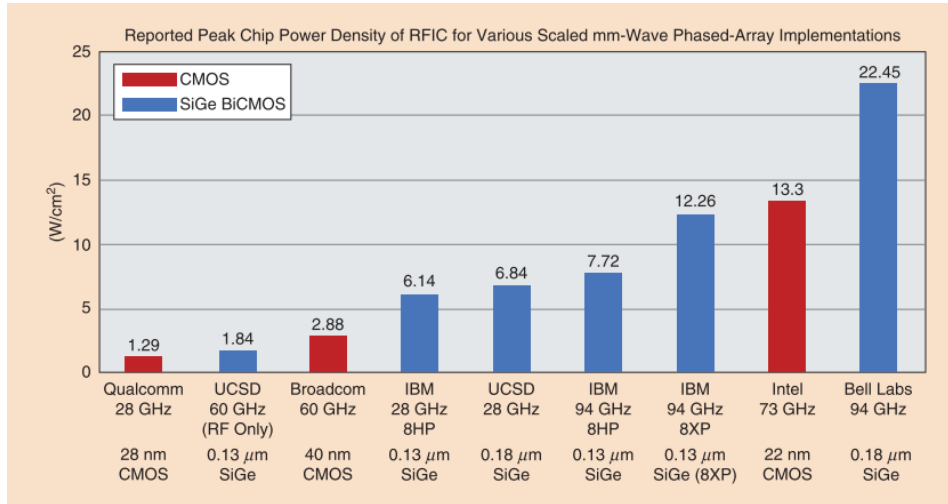


**Figure 1.2:** Comparison of IC power density in silicon based scaled phased array[11]

## 1.2. Latest research at MS3 on heatsink antennas

At MS3, Celik et al. introduced a co-design method for optimizing both the thermal and electromagnetic (EM) performance of a 3D patch antenna, as detailed in their publication.[12] The work is entirely simulation-based, utilizing ANSYS HFSS for the EM analysis and ANSYS ICEPAK for thermal simulations. However, dimensions and materials account for current manufacturing constraints and commercially available materials. Thermal simulation properties are defined by the junction-board thermal resistance ( $R_{jb}$ ) and junction-case thermal resistance ( $R_{jc}$ ), both sourced from manufacturer specifications.

The referenced antenna is a pin-fed patch with a shorted via wall at the center, as illustrated in Figure 1.3. It is designed to operate within the 24 GHz to 28 GHz frequency range, using Rogers RO5880 substrate ( $\epsilon_r = 2.2$ ,  $Tan\delta = 0.0009$ ) with a thickness of 0.254 mm, and copper for the conductive elements. Through parametric studies, three variations of heatsink fin designs were created and evaluated, as shown in Fig 1.4. The study details the effects of the orientation and spacing and orientation between the fins affect the effective length of the heatsink and, consequently, the operational frequency of the patch antenna. Fig 1.5 highlights the influence of fin proximity on the antenna's resonant frequency.

Thermal analysis, likewise, depicts the relationship between fin separation and angle, and heat dissipation. For instance, Antenna A dissipated 5° more heat from the chip than Antenna C, demonstrating the effect of spreading the fins on thermal performance, as shown in table 1.1 The heatsink base acts as a heat reservoir, drawing heat from the chip and distributing it across the fins. It is important to note, however, that there is a limit to how much heat the heatsink can extract. Heat extraction is governed by the number of shorting pins and the thermal conductivity of the chip's plate. Several benefits can be drawn from the insertion of the heatsink, however there are also several tradeoffs to be considered.

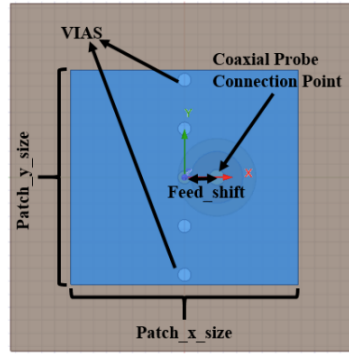


**Figure 1.3:** Pin-fed shorted patch design

	Chip Temp [°C]	Patch Temp [°C]	Heatsink Temp [°C]
Basic Patch	97.5	60.57	none
Shorted Patch	79.84	72.45	none
Antenna A	69.17	62.11	61.74
Antenna B	70.21	63.20	62.87
Antenna C	74.34	67.50	67.24

**Table 1.1:** Chip temperature per heatsink antenna topology

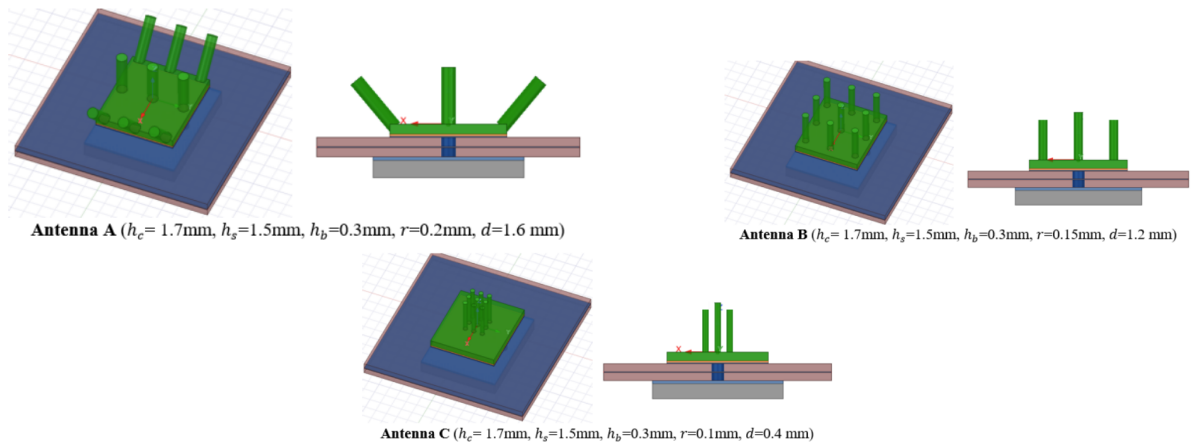


**Figure 1.4:** Fin heatsink antennas models proposed by the MS3 group[12]

## 1.3. Problem Formulation

Several key performance issues emerge from the analysis. One prominent issue is the narrow impedance bandwidth observed in Figure 1.5 across all heatsink configurations. This is largely attributed to the pin-feed method. While the addition of heatsinks enhances the inherently limited bandwidth of patch antennas by introducing an additional resonance, achieving broader bandwidths remains a critical goal.

Another significant challenge is the asymmetric radiation pattern introduced by the heatsink. The heatsink behaves as a hybrid of a patch and monopole antenna, increasing the potential for electromagnetic interference (EMI), which needs to be minimized.[3] A symmetric radiation pattern is highly desirable for active electronically scanned arrays (AESAs). Additionally, the placement of the heatsink fins impacts both co-polarization

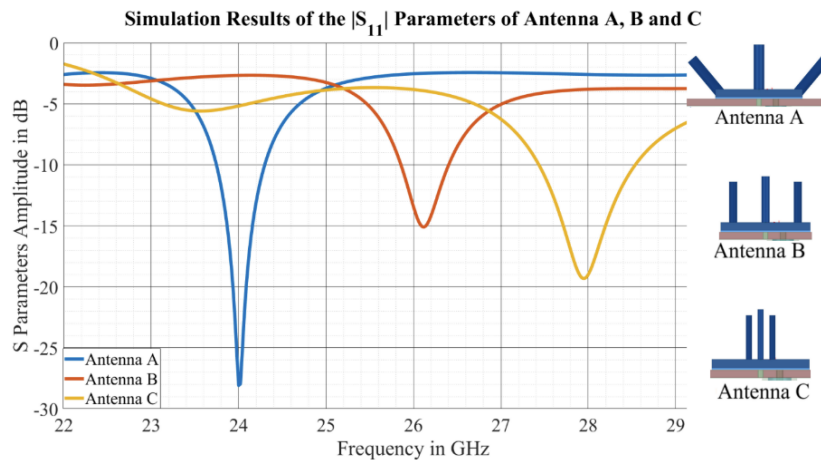


**Figure 1.5:** Heatsink antennas  $S_{11}$

and cross-polarization. When fins are positioned along the radiating edges of the patch, the radiation from the vertical fins becomes more dominant, which in turn influences the antenna's polarization. Moreover, this pattern distortion poses even greater challenges for patch antennas with phased array capabilities.

## 1.4. Objectives

As specified by section 1.3 the aforementioned issues require extra research. This work will attempt to overcome the EMI of heatsinks by introducing and analyzing the effects of differential feeding. The improvements will be benchmarked against the performance of the original work described in sections 1.2 and 1.3. The focus will be placed on metrics such as impedance bandwidth, realized gain, cross polarization level, radiation efficiency and radiation pattern symmetry for the element level. The resulting design will be analyzed at the element level as well as linear array level. Small considerations will be placed on heat dissipation capacity. Therefore to keep heat dissipation characteristics constant, heatsink design and shorting wall will be kept constant to provide a fair comparison. Therefore the key objectives of this works are the following:

- **Increase bandwidth achieved by initial heatsink patch through aperture coupling**
- **Reduce the EMI of heatsink antennas through differential feeding**
- **Analyze the radiation pattern metrics such as gain, main lobe angle, realized gain, 3db Beamwidth, and overall symmetry.**
- **Analyze the viability of a differentially fed heatsink patch antenna in a linear array.**

## 1.5. Scope

This work will be under the supervision of the MS3 group from TU Delft. It will be a follow up on the research done by the group in attempt to improve on their latest results on heatsink antennas. Said publication will also serve as a benchmark to compare the gain, radiation efficiency, co and cross polarization, radiation pattern symmetry and bandwidth. The main purpose of this work is to research a method to reduce EMI from

heatsinks, analyze its performance at the element level as well as a 1x4 linear array level. Frequency bands will be kept to the lower end of high band of 5G mm-wave. Therefore the target frequencies are between 26 GHz and 28 GHz. [13] **Antenna B** in figure 1.4 topology will be selected as the benchmark for this work. The work will be purely simulation based and will not consider manufacturing. However, manufacturing constraints, such as  $\epsilon_r$  and  $\tan\delta$  are taken into account in the design. Numerical simulations will be carried out using ANSYS Electronic Desktop HFSS 2023 R2.

## 1.6. Novelties

As far as the author of this work is concerned, this is the first time aperture coupling is proposed to improve bandwidth of a heatsink antenna. Likewise, it is the first time differential feeding is proposed to address heat sink radiation pattern distortions. Differential feeding provides a symmetric pattern due to its cancellation mechanism, as well as improved cross polarization levels in comparison to its single fed counterpart. Furthermore, the viability of its application in a differentially-fed linear phased array setup is analyzed. Additionally, for the first time the effects of amplitude and phase tapering on a heatsink patch element was analyzed. The effects on the radiation pattern at several angles as well as the possible applications of the tapering.

## 1.7. Thesis structure

This work will be structured as follows. **Chapter 2** gives a quick theoretical background for aperture coupling feeding technique. Furthermore, it delves into the latest research on differential feeding for patch antennas exclusively. **Chapter 3** Shows the gradual improvement of the patch heatsink antenna element. Introduces and compares the performance of aperture coupling and differential aperture feeding mechanisms against the benchmark. Further explores the potential capacity of single element beam steering of differential feeding. **Chapter 4** the resulting improved antenna element will be compared against the benchmark in a linear phased array setup. **Chapter 5** Summarizes, discusses and highlights the results and possible implications of this work. Future work is also discussed.

# 2

## Theoretical Background and Literature Review

In this chapter, an overview of the current state of research relevant to this work is given. a deep dive into the latest advancements in patch antennas, heatsink designs and feeding techniques will be carried out. The focus of the literature review will be on EM trade-offs of the aforementioned topics. Since the purpose of this work is to overcome the EM issues associated with heatsinks, a small consideration will be placed on thermal management. Furthermore, given the established reliability and extensive history of patch antennas, this literature review will not extensively cover their longstanding track record.

### 2.1. Theoretical Background

#### 2.1.1. Aperture coupled patch antenna feeding in patch antennas

Aperture coupling is a well known established patch feeding method, since it was introduced by D.Pozar in 1985.[14] It is a common feeding technique to improve bandwidth of an otherwise narrow bandwidth patch antenna.

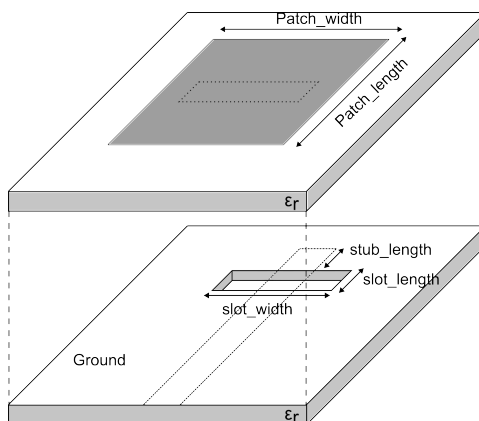


**Figure 2.1:** Aperture coupled patch parameters

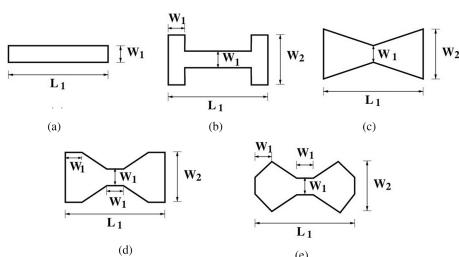
The transmission line is coupled to the radiating element via an aperture, enabling

efficient energy transfer without requiring direct electrical contact. This aperture is precisely etched into the shared ground plane separating the transmission line and the radiating element. This configuration ensures electromagnetic coupling between the two structures while maintaining physical isolation. The design is visually represented in Figure 2.1, which details the feeding scheme utilizing a microstrip line to deliver energy to the radiating patch.

The performance of the aperture-coupled patch antenna is heavily influenced by several design parameters associated with the feeding scheme. Proper optimization of these parameters is essential for achieving efficient impedance matching between the transmission line and the patch antenna. In this feeding technique, the length of the patch determines its resonant frequency, while the width of the patch affects the antenna's input resistance, both of which are critical for the antenna's overall performance. Additionally, the substrate thickness significantly impacts key performance metrics such as bandwidth and coupling efficiency. A thicker substrate generally improves bandwidth due to the reduced Q-factor of the resonator but simultaneously decreases coupling efficiency for a given aperture size, posing a trade-off for designers.

The aperture slot itself plays a central role in governing coupling characteristics. Among its dimensions, the slot width has the most pronounced effect on the level of coupling, influencing both the efficiency of energy transfer and the extent of back radiation. Figure ?? (a) illustrates the relationship between aperture size and coupling efficiency, showing how increasing slot width enhances coupling up to a certain point. While the length of the slot also affects coupling, its influence is much less significant compared to the slot width, with most designs employing a typical width-to-length ratio of approximately 1:10 to optimize performance.

Beyond basic coupling considerations, aperture coupling offers significant advantages in terms of electromagnetic isolation. The ground plane acts as a barrier, reducing spurious radiation from the feed network and minimizing mutual coupling in antenna arrays. This isolation is particularly beneficial in multi-element systems where cross-coupling can degrade performance. Furthermore, aperture coupling allows for advanced polarization designs. By altering the shape or orientation of the aperture slot (e.g., rectangular, cross-shaped, or H-shaped), the antenna can be configured for linear, circular, or dual polarization. Slots can also come in different shapes as illustrated in Figure 2.2. Although all shapes improve bandwidth, each shape provides different extra properties. Rectangular slots produce a linear polarization when positioned symmetrically with the radiating element. Circular slots distribute energy more evenly while also suppressing back radiation. H-shaped, or other more complex geometries can provide higher degree of coupling and bigger bandwidth, but may come with the trade off of higher back radiation. [15][16] This flexibility is especially valuable in applications like satellite communications and radar, where polarization diversity is critical.



Another critical parameter is the stub length, defined as the excess length of the microstrip line extending beyond the aperture slot. This stub serves to tune the reactive impedance introduced by the cou-

**Figure 2.2:** Slot shapes

pling mechanism. In most practical designs, the stub length is kept below  $\lambda/4$  to ensure effective compensation of reactive components. The impact of stub length on antenna performance is depicted in Figure 2.3 (b), which highlights its role in fine-tuning the

antenna's impedance response.

Aperture coupling also facilitates the use of multiple substrates, each tailored for a specific function. A high-permittivity substrate can be used for the feed network to confine fields and reduce radiation losses, while a low-permittivity substrate supports the radiating patch to enhance efficiency and bandwidth. This dual-layer configuration simplifies material optimization and enables multi-band or wideband operation by adjusting aperture dimensions or introducing multiple slots. The technique is also scalable, making it well-suited for phased arrays and active antenna systems where precise element control is required.

Finally, aperture coupling is compatible with a variety of transmission line topologies, including microstrip lines, stripline, coplanar waveguides, and substrate-integrated waveguides (SIWs). This adaptability, combined with its inherent performance advantages, makes it a preferred choice for modern antenna systems in applications ranging from communication networks to radar and sensing devices. By carefully optimizing the coupling parameters, designers can create high-performance, robust antenna systems tailored to diverse operational requirements.

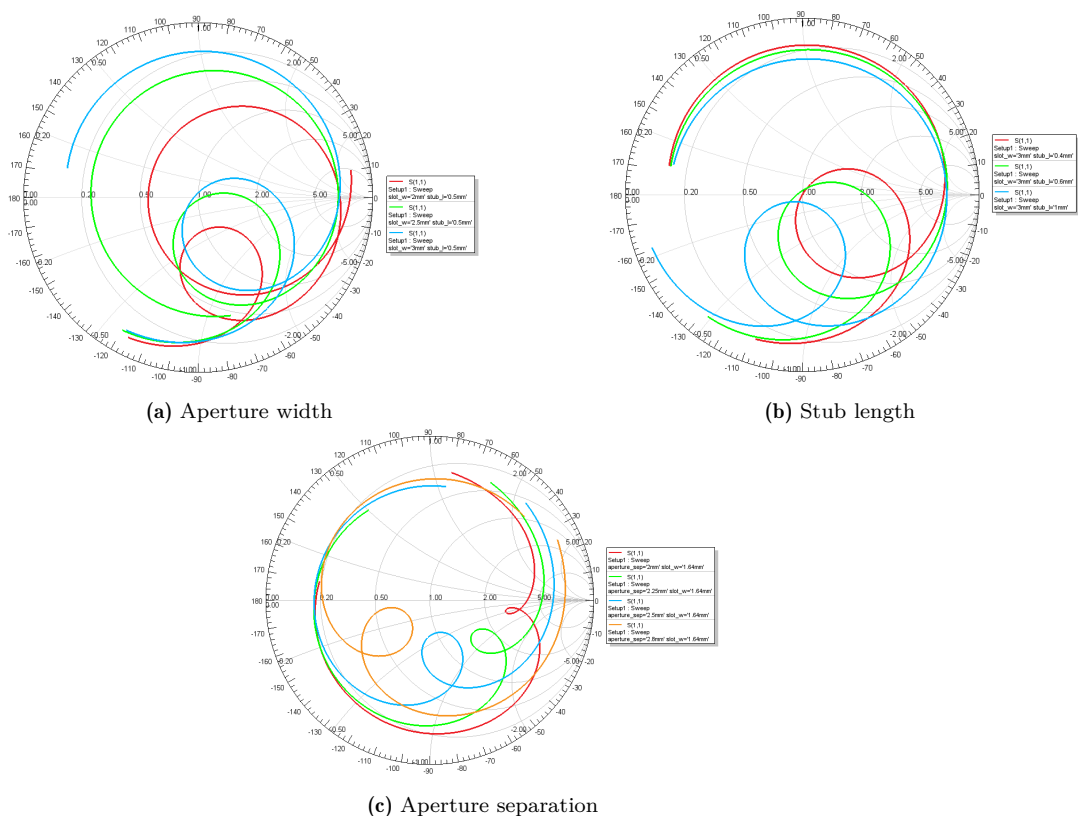


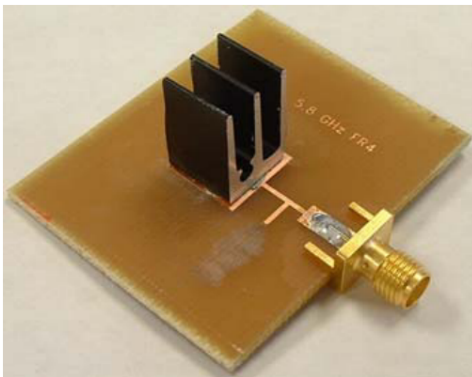
**Figure 2.3:** Effects of aperture width, stub length and aperture separation on coupling and bandwidth of a patch antenna represented on smith chart

## 2.2. Literature Review

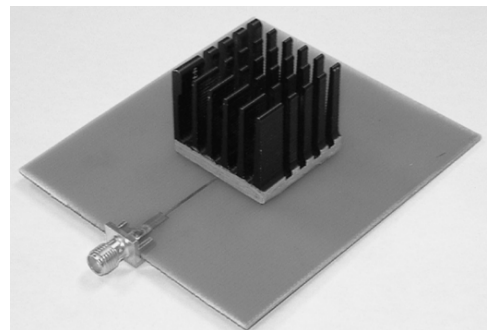
### 2.2.1. Heatsink Antennas

The concept of the heatsink antenna was first introduced by L. Covert in 2006. The proposed structure (shown in 2.4b) consisted of a patch antenna mounted on an FR-4 substrate, with a cut-up heatsink placed over the metal patch [9]. This design demonstrated improved radiation efficiency, leading to an increased peak realized gain from 2.46 dB to 4.12 dB. Simulations and measurements indicated that the resonant frequency of the antenna dropped by approximately 200 MHz due to the heatsink increasing the effective dimensions of the patch. Additionally, the heatsink reduced the S11 parameter at the input, compared to a basic patch antenna, by compensating for substrate losses. Furthermore, the heatsink introduced impedance mismatches but can be compensated with proper matching techniques.

Continuing to expand on this, L.Covert researches the implications of the orientation of extruded fins with respect to the radiating edges of a patch.[17] In this work it is clearly shown how aligning the extruded fins to the radiating edges of the patch plays an important role, specifically on the directivity and the radiation pattern. By adding the heatsink, the radiation efficiency improved by 20%, peak directivity gain almost 1 dB, and bandwidth was improved by 14% at 5.8GHz. It is important to note that the fins aligned with the non radiating edges demonstrated a better gain, bandwidth, and directivity than the heatsink aligned with the radiating edges



(a) Heatsink oriented along non radiating edges[17]



(b) First heatsink antenna design proposed by Covert[9]

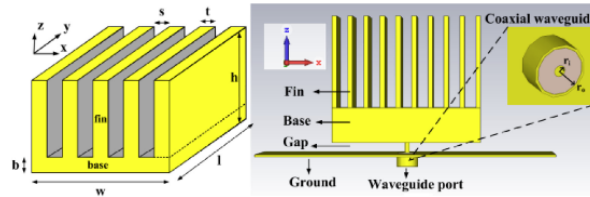
**Figure 2.4:** Antennas with heatsinks

**Fractal heatsink antenna designs** have also been explored. Casanova et al. investigated the effects of a 3D-printed fractal heatsink, which showed promising results in both heat management and electromagnetic performance [18]. The fractal structure consists of a cube of side length  $L$  and iteratively applying cubes of side length  $L/n$  centered on each corner. The side length of the cubes added in the  $n$ th iteration is  $L/n$ . The antenna heatsink is formed by bifurcating the total geometry above a substrate and ground plane. These bifurcations reduced thermal resistance as the number of fractal points were increased. Furthermore, the addition of fractal nodes also presented an increase of directivity and gain.

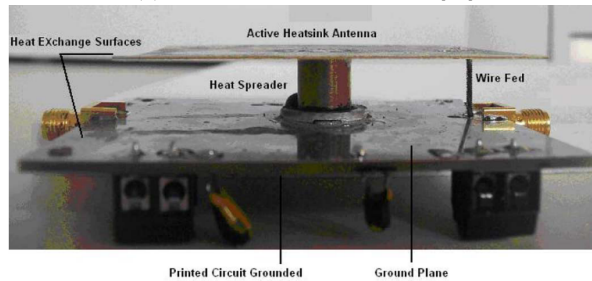
In a different approach, [19] investigates the direct application of an engineered **heatsink as an antenna**. The study applies conventional heatsink topologies to char-

acterize its EM performance. It is demonstrated that extruded fin heatsinks with a base act as a superposition of a patch and monopole antenna. Where the base dimensions determine the patch frequency and the fin extrusion length determines the monopole frequency.

[20] compliments the research on heatsink as an antenna. The antenna is elevated by a metal pillar that acts as a thermal spreader and support. The EM dimensions are calculated using the air as a substrate, which increases the surface contact with air to increase heat dissipation. Electrical wavelength of the patch rather large due to the relative permittivity of the air ( $\epsilon_r=1.0$ ).



(a) Elevated patch as heatsink.[19]



(b) Fin heatsink as antenna [21]

**Figure 2.5:** Heatsink as antennas

A **fin extruded heatsink adhered unto a patch antennas** for dual electro-thermal functionality [22]. In the study, the thermal and EM implications of the fin position and inclination angle are studied. Position and distance between the fins determines resonant frequency. It demonstrates an inverse relationship between fin separation and resonant frequency. Three different topologies of heatsinks are designed and benchmarked against patch antennas tailored to three frequencies in the high 5G frequency band (24 GHz -28 GHz). Shorting via wall was employed to ease heat transfer from the chip, through the antenna and into the heatsink. The via wall reduces temperature from the chip by almost 20°C, while the addition of the heatsink further reduces the temperature by an extra 10°C. While fin separation reduces the max gain, it does improve thermal performance.

A further advancement in the co-design of electromagnetic and thermal performance was proposed by Q. Jiawei, who introduced a **heatsink aperture antenna** with an open-ended waveguide array and extruded fins parallel to the H-plane of each antenna element [23]. The design featured metallic vias in the substrate integrated waveguide (SIW) feed network, facilitating both a transition between the substrate and the waveguide, and a more efficient thermal pathway from the chip to the fins. It is observed that the inclination of the fins can provide improved broadside gain by almost 2 dB but in turn reduced the beamwidth of the element. The radiation pattern of the elements showed a symmetric pattern, undisturbed by the extruded fins. Considering the fact that the fins

where not extended past a certain dimension to prevent them from supporting higher modes. Bandwidth achieved a 11.2% at 60GHz, with a gain of 9.84 dBi on its inclined fins.

In a similar approach, Zhang et al. addressed heating issues in Antenna-in-Package (AiP) systems by integrating a metal slab with **horn antenna slots** on the antenna side of the PCB [21]. This slab efficiently distributes thermal energy across the PCB to improve heat dissipation. This method did not include fins or any type of extrusion in order to prevent EM performance from deteriorating. The manufactured AiP achieves a bandwidth of 16% in the -10dB band with a max gain of 15.4 dB at 60GHz.

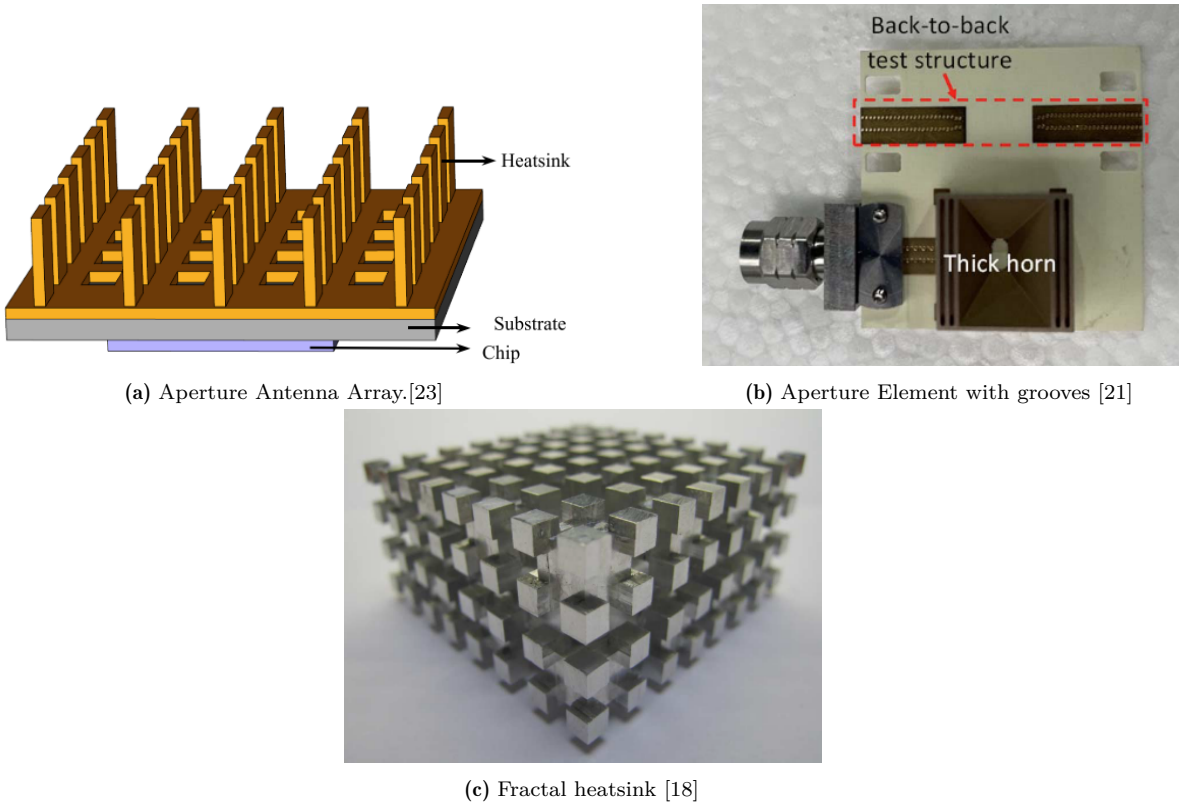


Figure 2.6: Aperture antennas with heatsink and fractal heatsink

### 2.2.2. Differentially fed patch

This section delves into various techniques and recent literature on differential feeding, a method that has gained prominence in antenna design. At the circuit level, differential feeding offers several performance advantages over single-ended feeding. In single-ended feeding, one side of the feed is grounded, whereas differential feeding employs two signals that are  $180^\circ$  out of phase. This configuration improves impedance matching, reduces common-mode noise, and enhances isolation. Additionally, differential feeding contributes to greater linearity and reduced offset, making circuits less sensitive to power supply variations, temperature fluctuations, and substrate noise compared to single-ended circuits. As a result, differential circuits are increasingly adopted in integrated circuit design [24]. This section will examine the trade-offs involved in designing differentially fed patch antennas.

An early comparative study by Zhang [25] explored the trade-offs between single-fed and differentially fed patch antennas. In it, it is demonstrated that the differentially fed patch antenna obtained a higher impedance bandwidth of 4.1% and a gain of 3.7 dBi, compared to the single-ended version with a bandwidth of 1.9% and a gain of 1.2 dBi. The differential patch also exhibited favorable co- and cross-polarization levels. Even under imperfect differential conditions, only the H-plane radiation purity was compromised. The study further revealed that initial design formulas for regular patch antennas are applicable to their differential counterparts. Although the patch length remains consistent for both single-ended and differential designs, the differential patch requires a wider width to ensure the excitation of the fundamental  $TM_{10}$  mode.

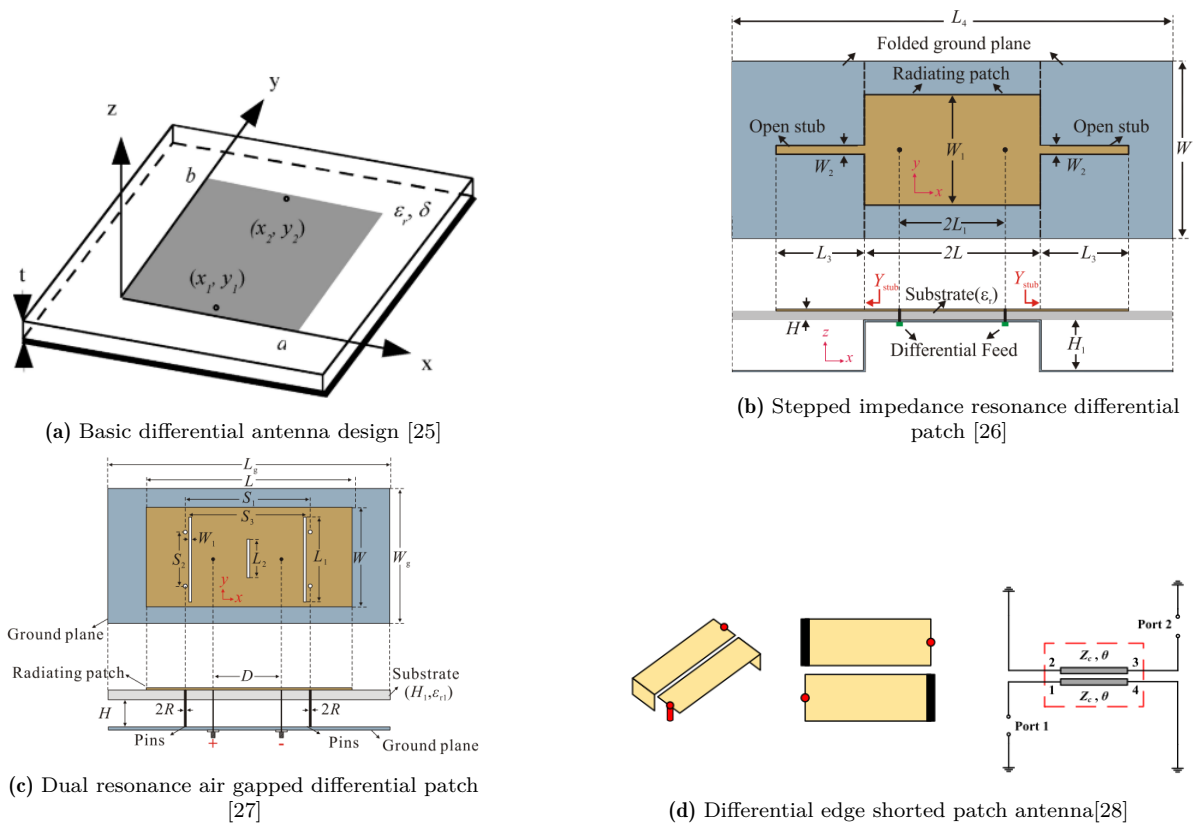


Figure 2.7: Differential patch antennas

Liu et al. [27] presented the use of an air substrate combined with a pin-fed differential antenna to achieve higher bandwidth and pattern symmetry. The bandwidth improvement was achieved by exciting dual modes and using a combination of shorting pins and etched slots to shift the resonances into the desired frequency band. This design resulted in a 13% bandwidth at 2 GHz and a stable radiation pattern. In an earlier iteration of their work, Liu et al. [26] employed a stepped impedance resonator to enhance bandwidth. By inserting stubs along the radiating edges and folding the ground structure beneath the stubs, they achieved a 10% bandwidth (from 0.84 to 0.94 GHz) with stable broadside gain of 8 dB and low cross-polarization.

While these studies demonstrated the benefits of differential feeding in terms of bandwidth enhancement, they also highlighted the increased patch size needed to reduce coupling between ports. However, Shao et al. [28] showed that this size increase is not always necessary. By etching a slot between the two differential ports, the patch length was reduced to shorter than  $\pi/2$ . This shortening was explained using a modified transmission line model. Although this design resulted in a narrower bandwidth (50 MHz at 2.20 GHz) and lower radiation efficiency, it provided higher directivity and a more symmetrical radiation pattern.

[29] takes another approach to reduce the differentially driven antenna size based on capacitive slots. The patch antenna works in half mode by loading shorting pins on the edges of the patch. Furthermore, the author added extra reduction mechanisms through the insertion of a slow-wave structure in the middle of the antenna as well as parasitic strips on the sides. With miniaturization reaching a 90.6%, peak gain reached 2.7 dB. Radiation pattern kept a very symmetrical pattern due to the differential excitation. Cross polarization levels for E and H fields achieved -19.7 dB and -18.7 dB respectively. Impedance bandwidth only reached 15 MHz at 2.4 GHz.

One of the main reasons engineers have historically avoided differential designs is the complexity of the feeding networks, which are far more intricate than those used in single-ended systems. Differential feeding typically requires the use of lossy baluns or other complicated feeding schemes, adding to the complexity of the layer stack-up.[24] This complexity becomes even more pronounced when trying to achieve **dual polarization in a differential scheme**. However, several studies offer solutions to simplify these feeding schemes for dual polarization. For instance, [30] suggests implementing dual polarization through vertical transitions in a stacked patch design. By using cross-shaped strips as feeding lines and connecting them to the patch via four slots etched in the middle layer, the author achieves a compact structure with a fractional bandwidth of over 19% and strong isolation ( $S_{dd21} = -35$  dB) between differential ports across the operational band. Additionally, the study proposes a method to convert single-ended S-parameters into differential port measurements

$$S_{dd11} = 0.5 \times (S_{11} - S_{12} - S_{21} + S_{22}) \quad (2.1)$$

$$S_{dd22} = 0.5 \times (S_{33} - S_{34} - S_{43} + S_{44}) \quad (2.2)$$

$$S_{dd21} = 0.5 \times (S_{31} - S_{41} - S_{32} + S_{42}) \quad (2.3)$$

$$S_{dd12} = 0.5 \times (S_{13} - S_{14} - S_{23} + S_{24}) \quad (2.4)$$

In another dual polarized approach proposed by [31]. The design consists of a theoretical dual aperture coupled feed with  $180^\circ$  phase shift.

[32] presents a dual polarized patch scanning array for weather applications. A differential feed is used to suppress cross polarization in the vertical excitation along with an imaged feed for the horizontal excitation. Array radiation pattern measurements showed a  $> -10\text{dB}$  cross polarization levels for the differential feed and a symmetric pattern for the element and the array setting.

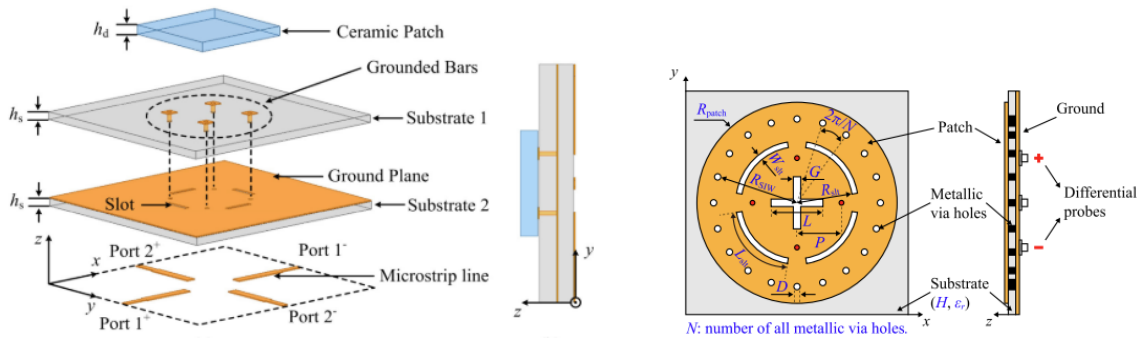


Figure 2.8: Differential dual polarized aperture coupled

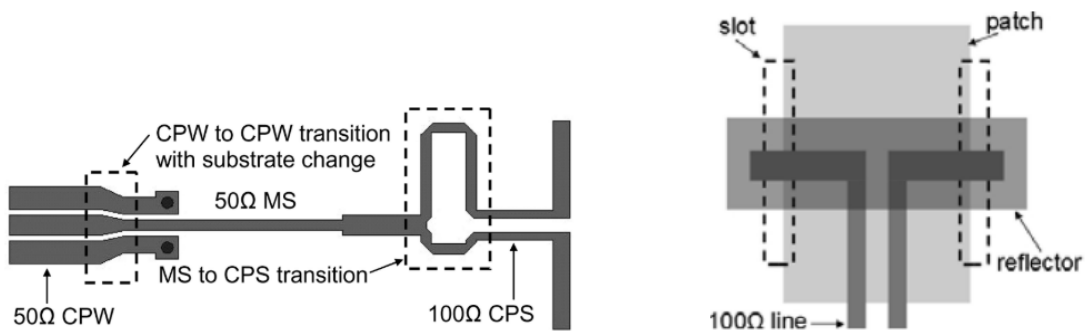
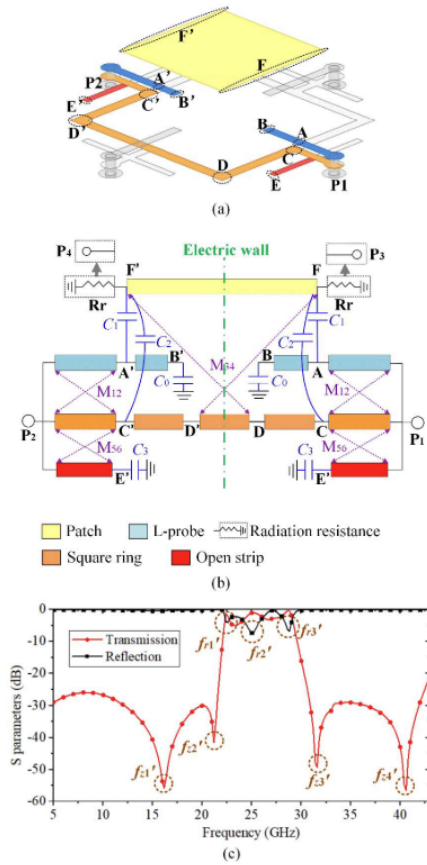


Figure 2.9: Differential aperture coupled feeding scheme

A low cost, high gain **differential array** for AiP purposes was designed by [33]. The element and array is design on a low cost pcb process at 60 GHz resonant frequency.

Differential feeding with aperture coupling is used to improve bandwidth as well as maintain a symmetric pattern with low cross polarization. The element peak element gain reached 8.91 dB and a impedance bandwidth of 12 GHz. Two array topologies were simulated and manufactured, one with fixed beam and one with digital beam scanning. The array successfully integrated each by using a power splitter with  $180^\circ$  phase shift line, converting from single line to differential feeding for each element. Taking advantage of the inherent short wavelengths at 60 GHz, the transition from single to differential does not become a mayor issue for integration. The array with digital beamsteering was capable of maintaining a 16 dB gain when scanning an angle of  $30^\circ$ .

Similar feeding scheme was proposed in an earlier design by [34]. The differential antenna array design proposed for 60 GHz. The proposed design was also implemented for AiP solutions.



**Figure 2.10:** [35](a)Antenna element (b)Equivalent circuit (c) Filtering capabilities

Similar performance as the earlier array was reported. Measurements report a peak antenna gain of 8 dBi, a -10 dB bandwidth of approximately 10 GHz and a radiation efficiency of 80%. The 16 element array achieved a 17 dBi on the broadside. The author mentions the suitability of the manufactured array in fixed beam as well as digital beam-steering setups. Some issues identified on the study is the heightened complexity as well as the increased dimensions of the array.

[35] seen in figure 2.10 proposes a dual polarized patch array element with filtering capabilities for 5G applications. A differential L stub feeding is used to provide a symmetric pattern and filtering response to each array element. The dual Additional square ring and open strips are connected to each probe, resulting in radiation nulls and realizing the lower/upper stop-band rejection level over 24 dB with skirt selectivity. The differential feeding network in the design ensures high isolation between the polarization states, leading to better performance in terms of polarization purity. This minimizes cross-polarization interference. The paper acknowledges that the differential-fed design adds complexity to the feeding network. The authors solution involves intricate feeding schemes that can increase design and fabrication challenges.

## 2.3. Conclusions

### 2.3.1. On heatsinks

Heatsinks demonstrate a clear improvement in thermal management; however, they introduce trade-offs in electromagnetic (EM) performance. Radiation efficiency improves in nearly all scenarios, while bandwidth depends on the heatsink's dimensions and topology. It is important to note, however, that the symmetry of the radiation pattern is consistently affected by the commonly used fin extrusion heatsinks.

One approach to achieving a seamless integration between antenna and heatsink involves adopting a horn-fin extrusion heatsink design, as proposed by [21] and [23]. While these designs yield highly promising results, they are expensive and demand advanced manufacturing capabilities. Similarly, custom designs like the fractal heatsink introduced by [18] face scalability challenges due to the complexity of their topology.

Given these constraints, the use of standard fin extrusion heatsinks currently represents the most practical solution, balancing cost-effectiveness with acceptable performance trade-offs.

### 2.3.2. On differential feeding

Differential feeding has clear advantages over its single ended counterpart. It has the capacity to improve bandwidth, as shown by [26] [27], radiation pattern symmetry and reduce cross polarization levels was demonstrated across all the literature available. While differential feeding has clear benefits most of the studies emphasize the increased complexity of the network. Due to manufacturing imperfections, it may prove too difficult to implement in large-scale commercial applications without further simplification. Moreover, the large scale of the antenna size may also affect the integrability in 5G applications. However, this complexity is tied to the required and manufacturing constraints, therefore as we move to higher frequencies, it may prove beneficial to move to a differential feeding scheme.

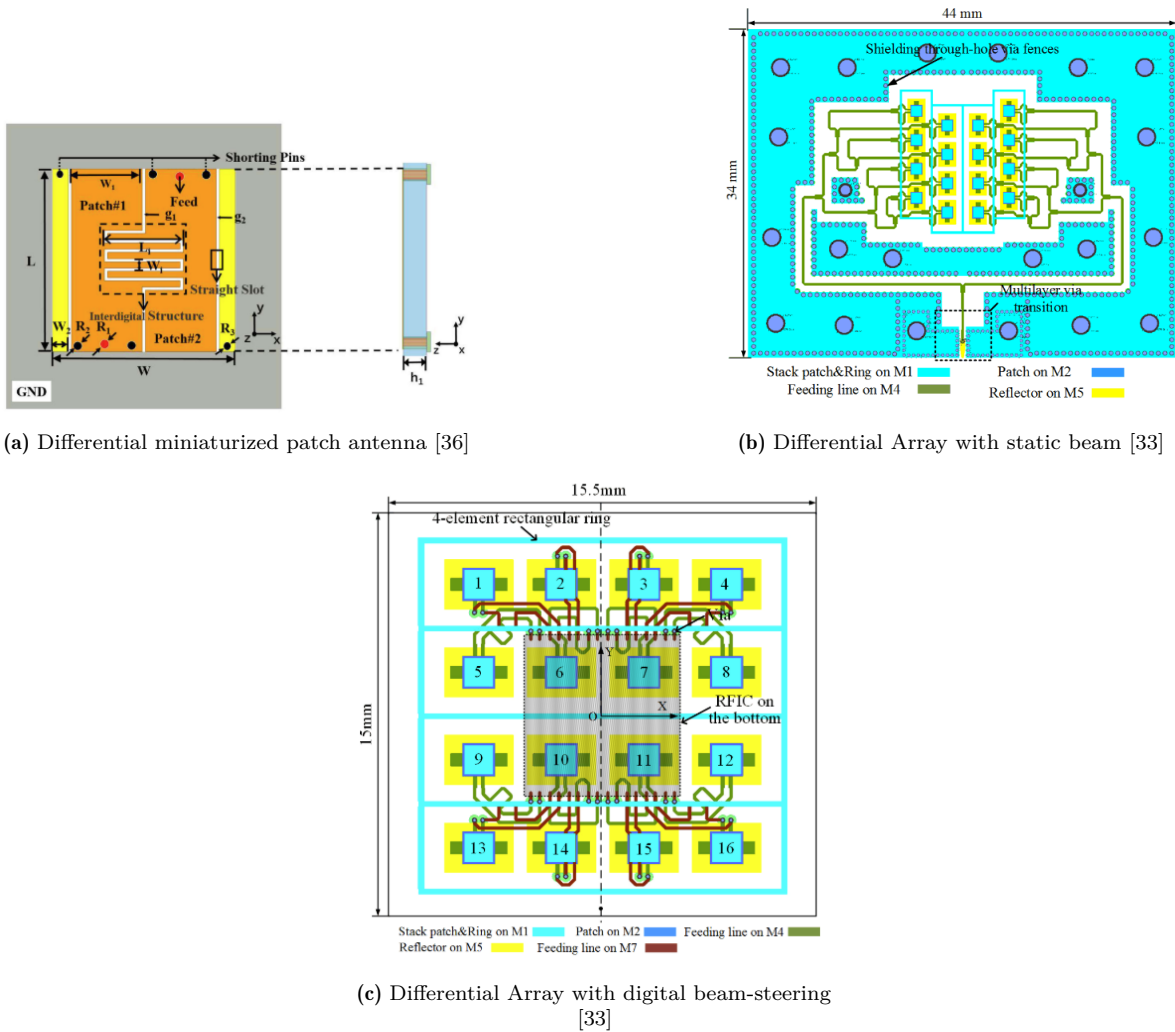


**Figure 2.11:** Differential patch antennas

## Heatsink Antenna Element

### 3.1. The benchmark- Pin fed heatsink antenna model

A model of the latest heatsink antenna model is replicated and simulated. The model is used as a benchmark. The heatsink is modeled to precisely match the dimensions of **Antenna B** in figure 1.4[22] for 26 GHz center frequency. The antenna consists of a shorted patch antenna with a heatsink attached at the top. The substrate material used is RO5880 ( $\epsilon_r = 2.2, \tan\delta = 0.0009$ ), with a standard Rogers thickness of 0.254 mm. Copper metal is used for the patch, ground, shorting pins and coaxial pin. The coaxial feed consists of a copper pin covered by Teflon ( $\epsilon_r = 2.1, \tan\delta = 0.001$ ) and grounded by a metal cover.

Heatsink is a fin extrusion heatsink with nine cylindrical fins. Three fins on each radiating sides of the patch measure to 1.5 mm height while the middle section reaches 1.7 mm. Radius of the cylindrical fins are 0.15 mm and they each have a 1.2 mm radius of separation between the adjacent fin. The base of the heatsink is a square metal patch with a thickness of 0.3 mm. The heatsink is attached by an FR4 epoxy glue ( $\epsilon_r = 4.4, \tan\delta = 0.02$ ) with a thickness of 0.05 mm. Five shorting vias are placed in the middle of the patch parallel to the radiating edges. The vias are separated equally by 0.65 mm from edge to edge. The coaxial pin is offset from the middle by 0.5 mm. The element ground length at all sides are the kept at  $0.5\lambda$ .

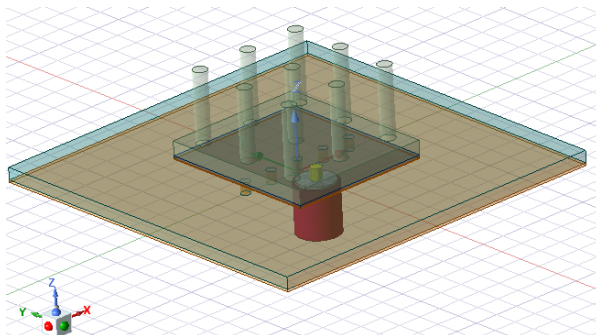


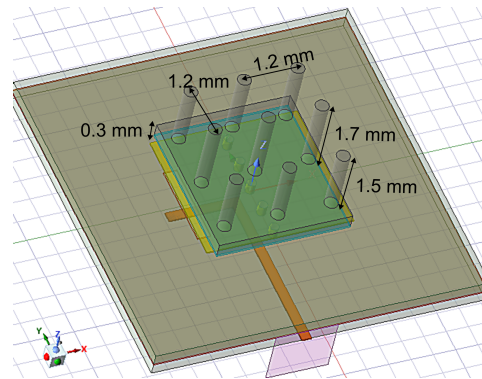
**Figure 3.1:** Pin fed patch with heatsink [benchmark]

### 3.2. Aperture coupled patch model with and without heatsink

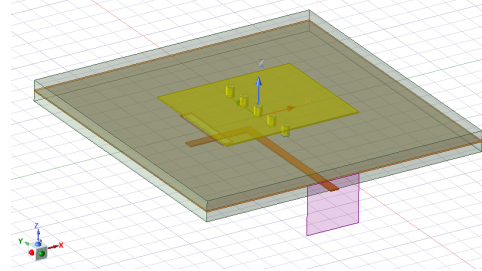
An aperture coupled patch is designed to improve bandwidth of the original pin fed. To ensure a fair comparison, several parameters are maintained constant. Substrate thickness and material are kept the same. Length, width and thickness (3 mm, 3.3 mm and 0.3 mm respectively) of the heatsink base are kept. Five shorting pins to the patch are maintained to keep thermal performance consistent, as shown in figure 3.2.

Two substrates separated by a ground plane with an aperture are required. For the bottom substrate, which carries the signal from the waveport to the aperture, Rogers TMM10 ( $\epsilon_r=9.2$ ,  $\tan\delta=0.0022$ ) is used. A high permittivity substrate is used to reduce dimensions of the transmission line. The feeding line is bent by 90 degrees to ensure the edge port does not align with the patch surface currents. This, consequently allows for phased array analysis. The microstrip line is tailored to  $50\Omega$  with a waveport feeding type.

The aperture is a regular rectangular slot with 1.64 mm in width, and 0.3 mm in length. The aperture is offset by 1.4 mm from the center to match the  $50\Omega$  impedance of the line to the patch antenna.



(a) Single feed aperture coupled patch with heatsink



(b) Single feed aperture coupled patch without heatsink

**Figure 3.2:** Single aperture coupled patches with heatsink (a), and without heatsink (b)

## 3.3. Differential aperture coupled patch

### 3.3.1. Power divider design

A simple Phase shifted power divider (PSPD) was designed to provide an approximate 180 phase shift and equal amplitude for an element. The width of the circuit is constrained to the length of the patch, to provide symmetry on both sides of the element for array analysis. A T-junction is a widely used power divider topology due to its simplicity in design and ease of impedance matching, making it ideal for early-stage differential feeding designs. It typically divides power in a 1:2 ratio across its output ports. The phase shift of 180 degrees is added by increasing the length of one output ports of the power splitter. The inherent losses in the substrate make it harder to achieve a perfect division on each port. Power and phase difference was calculated by substrating  $S_{21}$  and  $S_{31}$  with their respective angle and power units. The best power balance achieved was 1 dB with. Output variables defined in HFSS are as follow:

$$\Delta\phi = \text{abs}(\text{db}(S(2, 1)) - \text{dB}(S(3, 1))) \quad (3.1)$$

$$\Delta\text{Power} = (\text{db}(S(2, 1)) - \text{dB}(S(3, 1))) \quad (3.2)$$

A look at the  $S_{11}$ , phase shift and power difference, shows the performance of the PSPD. Bandwidth is relatively lower compared to an ideal T-junction. The bends of one of the ports reduced the resulting bandwidth as well as the imperfect transformation of single ended to differential impedances. However, the bandwidth satisfies the operational frequency of the patch antenna. Phase shift also is kept within a reasonable 3 degrees difference at 26 GHz.

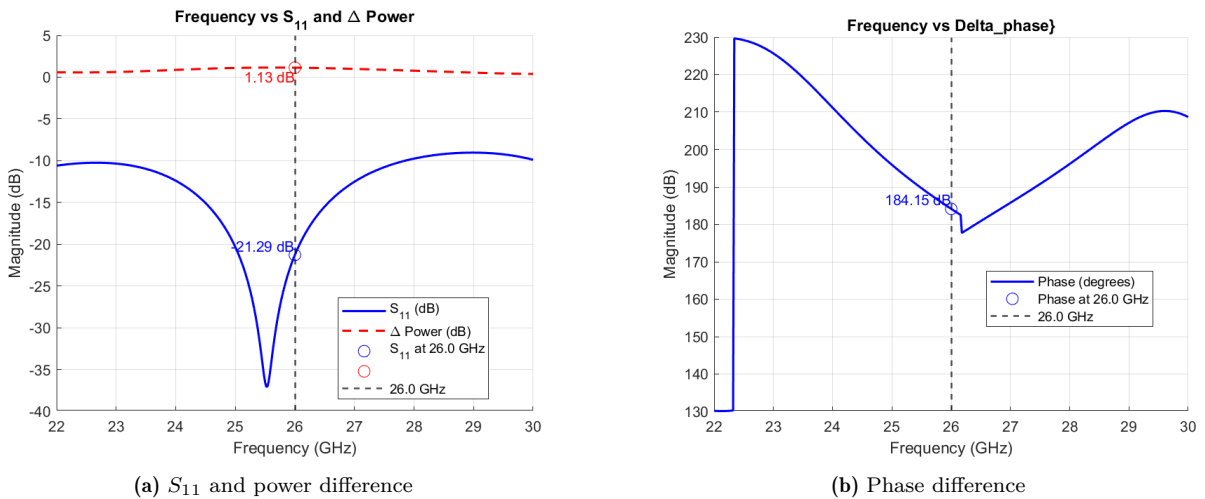
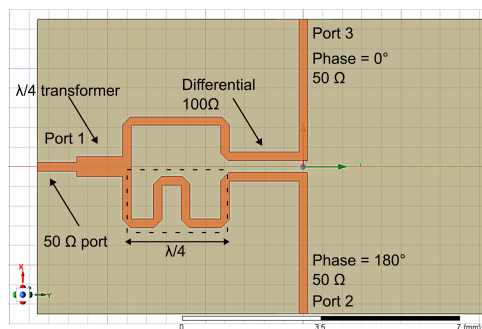


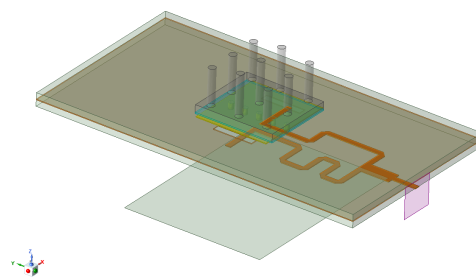
Figure 3.3: PSPD performance

### 3.3.2. Differentially fed patch element

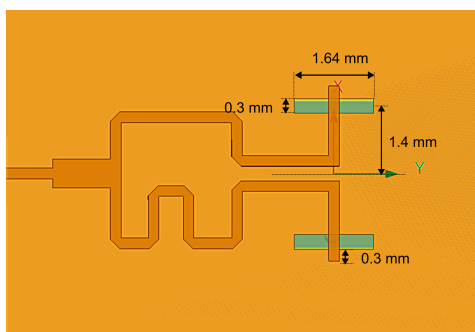
Using the PSPD, differential feeding scheme is introduced for the patch element. With the addition of differential feeding, small adjustments in the patch element must be made. Patch length and width are kept the same. However small changes to the aperture position with respect to the middle of the patch length are made. Aperture width reduces to 1.6 mm. Single feed aperture is positioned at 3 mm from the middle, whereas the differential apertures are located at 2.8 mm each. The stub length varies ever so slightly by 0.1 mm longer on the single element than in the differential element. An extra substrate length is added on the +Y axis to compensate for the extra length added by the PSPD.



(a) PSPD bottom view



(b) Differential aperture coupled heatsink antenna with reflector



(c) Bottom view PSPD with slot spacing and dimensions

**Figure 3.4:** Differential heatsink antenna and PSPD

## 3.4. Single elements results

### 3.4.1. Aperture Coupling Performance and the Impact of Heatsink Integration

Aperture coupling demonstrates a significant improvement in bandwidth compared to pin feeding, increasing the bandwidth from 500 MHz to 1 GHz while maintaining the same substrate thickness. Moreover, the inclusion of a heatsink further enhances the bandwidth. As shown in Figure 3.5, removing the heatsink results in a noticeable reduction in operational bandwidth. This enhancement is attributed to the heatsink dimensions, which are closely aligned with the resonant frequency, effectively broadening the operational bandwidth.

However, while the bandwidth improvement is a clear advantage, it comes at the cost of substantial degradation in the radiation pattern. Figure 3.6(a) illustrates that the radiation pattern of a patch with and without heatsink. The radiation pattern exhibits a null at  $50^\circ$ , a main beam offset by  $-11^\circ$ , and an undesirable lobe at  $90^\circ$ . The lobe at  $90^\circ$  is likely due to the monopole-like behavior introduced by the heatsink fins. Additionally, the maximum gain is reduced by approximately 3 dB when transitioning from pin-fed to aperture-coupled feeding with a heatsink. Removing the heatsink from the aperture-coupled patch results in a slight gain increase of 0.5 dB, suggesting that aperture coupling is more susceptible to distortions introduced by the heatsink. Furthermore, a high level of cross-polarization is observed, with the maximum cross-polarization for a single aperture-coupled patch with a heatsink reaching as high as -7 dB. Figure 3.6b further emphasizes these issues, showing a 3D radiation pattern with the null at  $50^\circ$  and a tilted monopole-like shape, indicative of heatsink-induced effects.

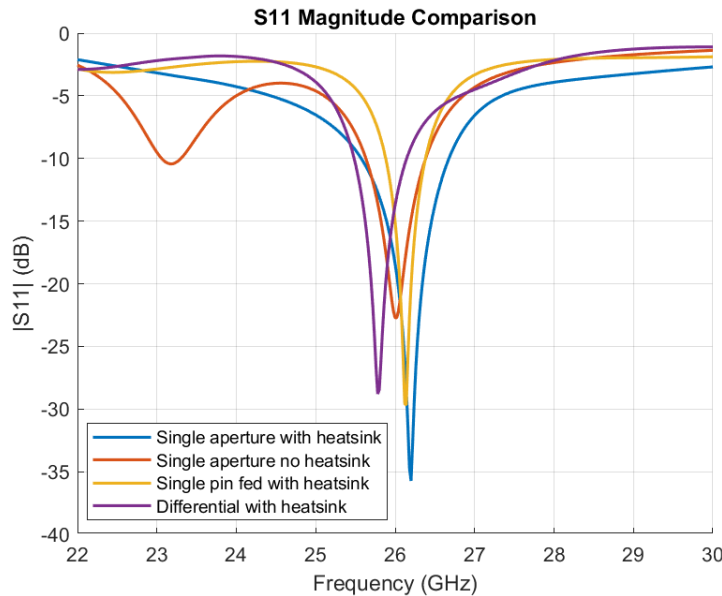


**Figure 3.5:**  $S_{11}$  comparison between single aperture without heatsink, single aperture with heatsink and Pin fed with heatsink.

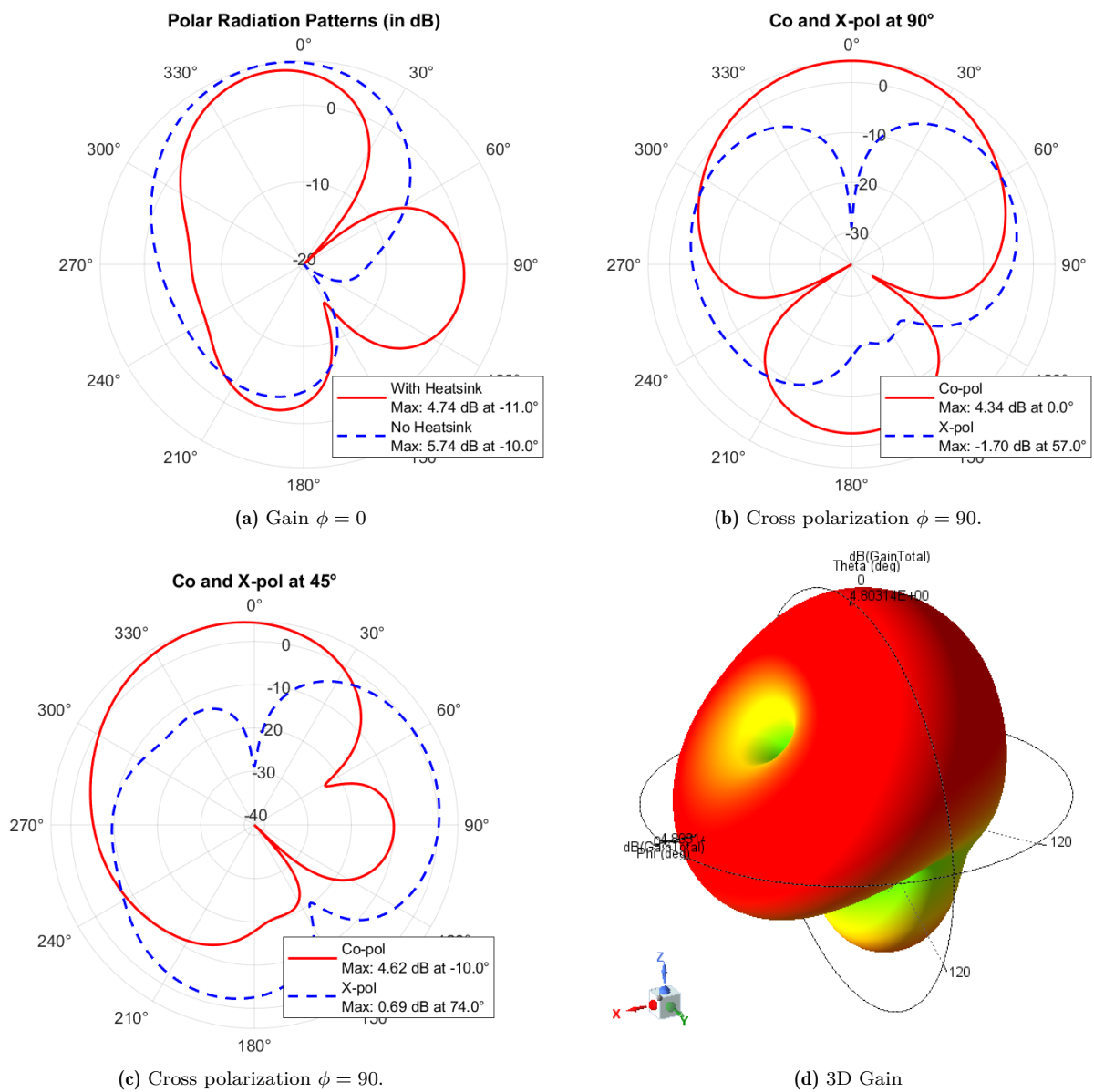


**Figure 3.6:** Aperture coupled patch with heatsink

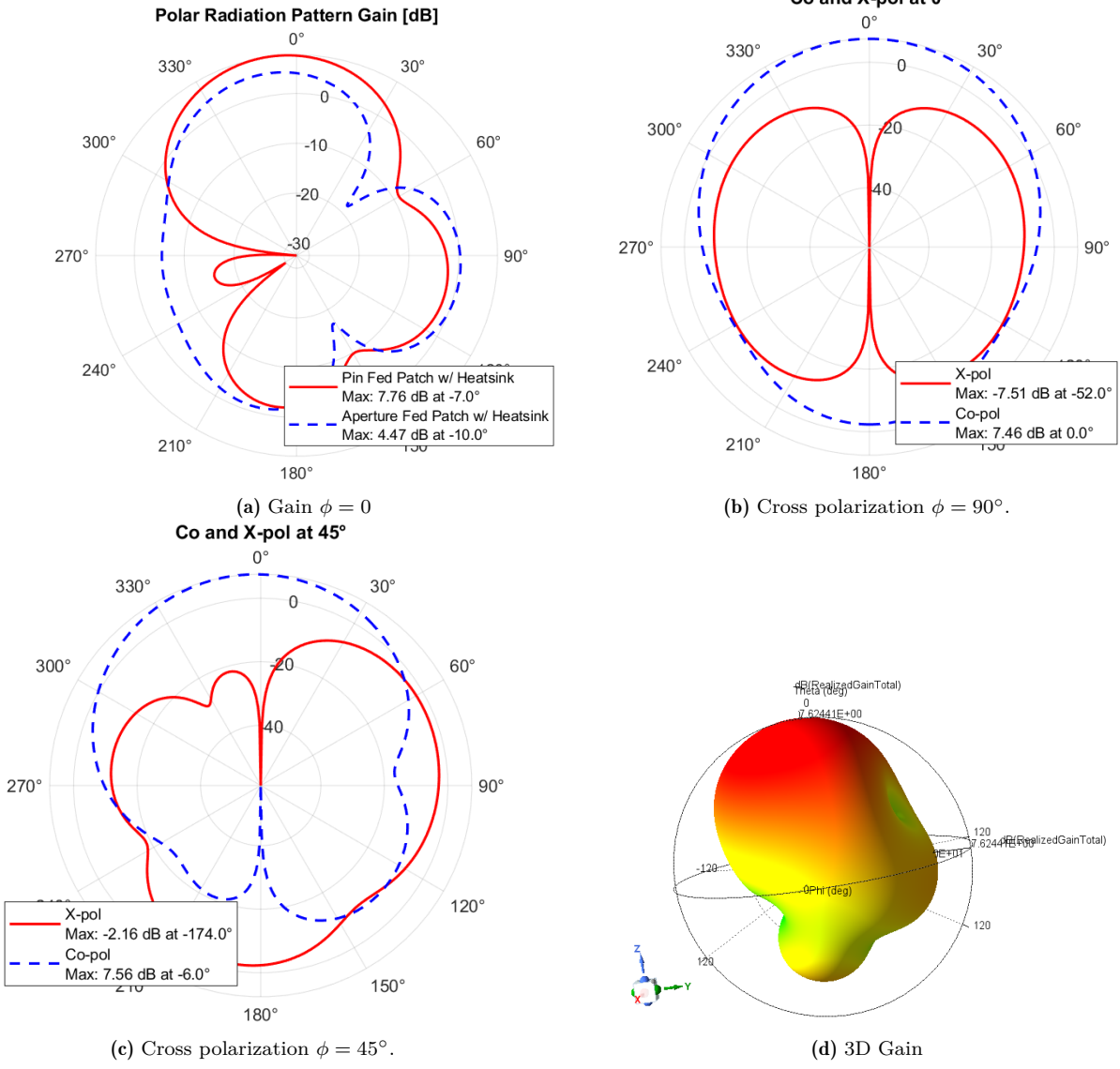
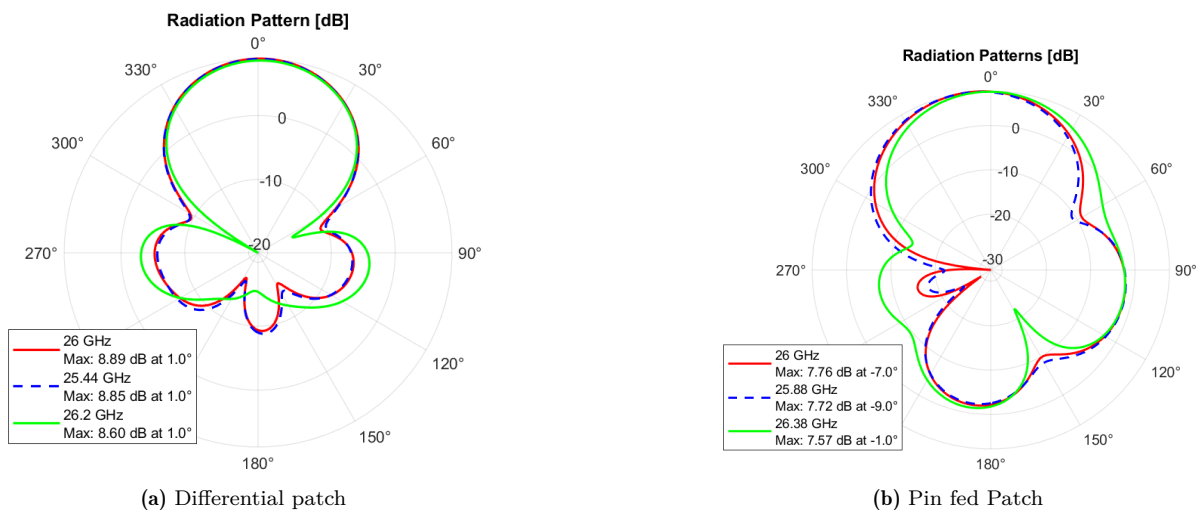


Figure 3.7: Pin fed patch patch with heatsink

### 3.4.2. Differential Feeding Integration Results

Introducing differential feeding yields interesting results. Bandwidth is reduced compared to a single aperture-coupled patch, decreasing from 1 GHz to 740 MHz. While this represents a degradation in bandwidth performance, it still surpasses the 500 MHz bandwidth achieved by the pin-feeding method. However, the radiation pattern shows remarkable improvements with differential feeding. The maximum gain reaches an impressive 8.8 dB, with a realized gain of 8.7 dB. Additionally, radiation pattern symmetry improves significantly, as shown in Figure 3.9, where the dipole-like behavior caused by the heatsink fins is notably absent. Back radiation is relatively high, and might affect the overall gain. Therefore, a metal reflector was positioned at  $\lambda_0/4$  from the radiating microstrip. The results suggest that differential feeding effectively mitigates the dipole resonance introduced by the heatsink fins, leading to a symmetric radiation pattern. However, the additional bandwidth provided by the heatsink is sacrificed. The radiation pattern also demonstrates a narrower beamwidth at  $\phi = 90^\circ$  compared to the benchmark. The 3-dB beamwidth is reduced to  $64^\circ$  for the differentially-fed configuration, compared to  $78^\circ$  for the pin-fed configuration. At  $\phi = 0^\circ$ , beamwidth remain relatively similar across feeding methods. It is also interesting to note that differential feeding offers a symmetric pattern across the radiation bandwidth. As shown in 3.8, the pin fed patch shows inconsistent radiation pattern as well as a deviation on the main beam. However, differential feeding keeps a consistent radiation pattern throughout as well as the main beam angle. The one degree deviation in differential feeding can be attributed to the imperfections in the PSPD, creating imbalances in phase and amplitude.

This imperfection raises questions regarding the effectiveness of beam-steering in a single element and the extent to which it can be achieved. To explore this, a parametric study was conducted on amplitude and phase tapering applied to a single element. The results, detailed in Appendix A, show that gradually increasing the amplitude imbalance between ports induces various phase shifts. The corresponding  $S_{11}$  parameters for both ports were plotted, with the analysis focusing on the overlapping impedance bandwidth below -10



**Figure 3.8:** Radiation bandwidth comparison between Differential patch (a) and Single Pin fed Patch (b).

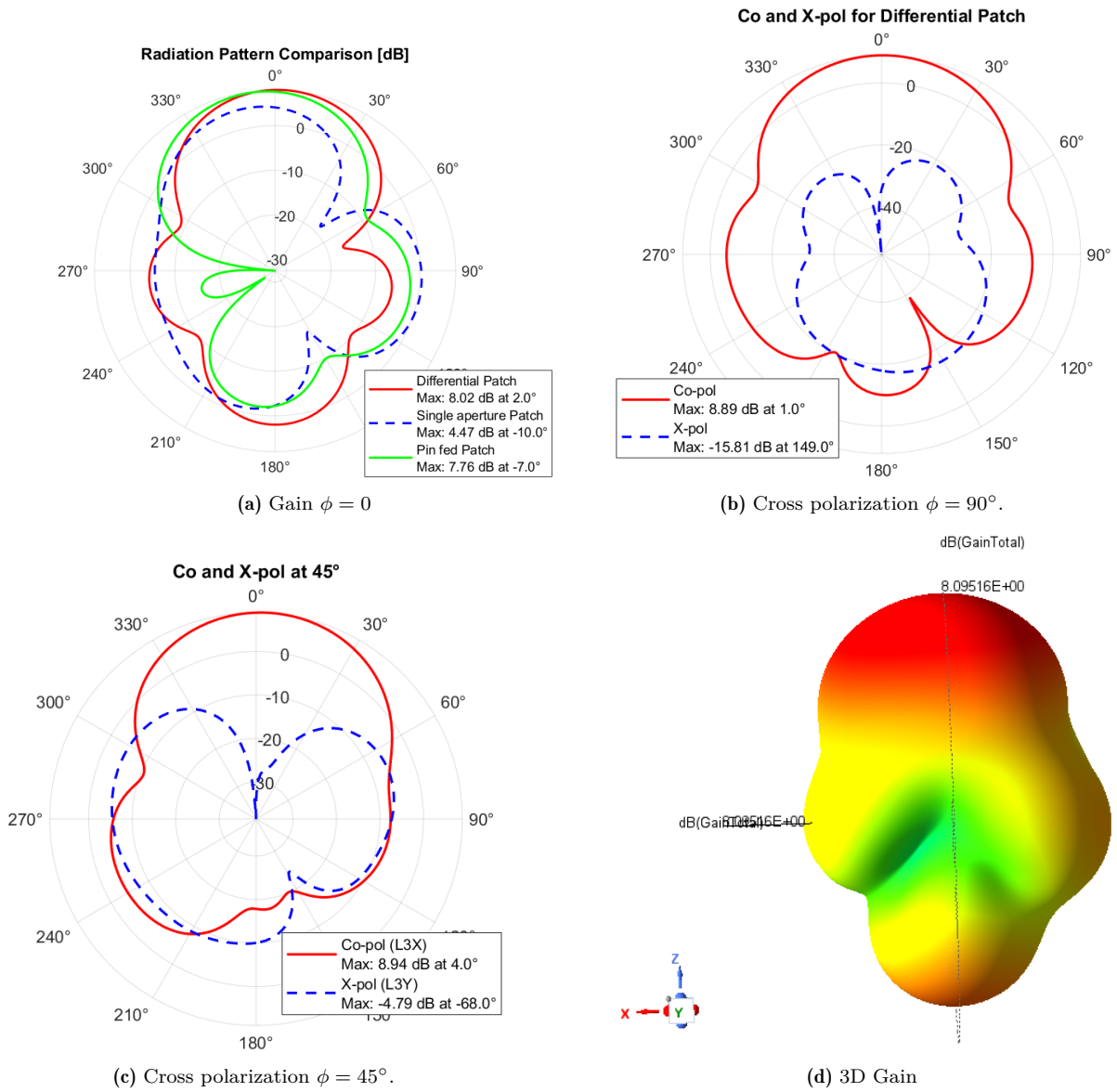


**Figure 3.9:** Differentially fed patch with heatsink

dB. Green labels indicate cases where both impedance bandwidths overlap, while red labels denote cases where only one or none overlap.

Although beam steering by approximately  $\pm 8^\circ$  is theoretically possible, the phase shifts that maintain a -10 dB overlap are constrained to  $\pm 1^\circ$ . Consequently, rather than achieving significant beam steering, the beamwidth angle increases under these conditions. The parametric study highlights that phase variations have a more pronounced effect on the radiation pattern than amplitude variations. The imbalance analysis was performed for one side only, as results for the inverse case were found to be symmetrical.

# 4

## Differential Array Design

### 4.1. Linear array differential differential and pin feed considerations

A four element linear array was designed and simulated for both differential fed patch with heatsink, as well as pin fed patch with heatsink. Both arrays without heatsink were also simulated. The elements are aligned along the orientation of the surface currents. Several spacings between elements ( $0.5\lambda = 5.88mm$ ,  $0.6\lambda = 6.9mm$ ,  $0.75\lambda = 8.66mm$ , and  $\lambda = 11.54mm$ ) were simulated to analyze the effects on impedance bandwidth, coupling and radiation pattern. Active S parameters are used to calculate the effective return loss as well as coupling of each element under excitation. A progressive phase shift ( $30^\circ$ ,  $60^\circ$ ,  $90^\circ$ ,  $120^\circ$ ) is applied to steer the main beam to several angles and observing the performance of the array. Main beam angle, beamwidth, grating lobes, side lobes and nulls of the radiation patterns are analyzed. Furthermore, Co and cross polarization are analyzed for orthogonal and  $45^\circ$  cutplanes. For co and cross polarization Ludwig3 coordinate system is applied to analyze in HFSS, with L3Y being the X-Pol and L3X being the Co-pol of the arrays.

### 4.2. Linear array results

#### 4.2.1. Impedance and Coupling Performance

Heatsinks increase coupling between elements, as evidenced by the *active*  $S_{11}$  results shown in Figures 4.2 and 4.3. At a spacing of  $0.5\lambda$ , there is significant coupling between elements, particularly affecting the middle elements more than the edge elements. However, as the spacing increases, the middle elements progressively achieve the minimum  $-10$  dB threshold.

For **pin feeding**, higher spacings demonstrate good performance but exhibit a narrow impedance bandwidth, as is typical for this feeding method. In contrast, the **differential feeding array** shows a substantial improvement in impedance bandwidth, reaching up to 1.8 GHz at  $\lambda$  spacing. Notably:

- At  $0.5\lambda$  and  $0.6\lambda$ , the pin-fed array achieves a better impedance bandwidth across

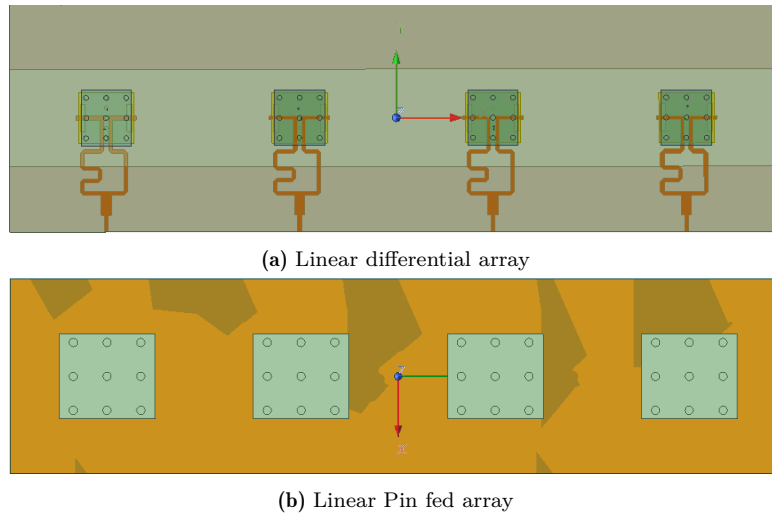


**Figure 4.1:** Four element shorted patch linear arrays (a) Differentially fed and (b) single pin fed with heatsinks, for phased array analysis.

all elements.

- At larger spacings ( $0.75\lambda$  and  $\lambda$ ), the differential feeding method outperforms the pin-fed array, achieving an improved impedance bandwidth of up to 2.2 GHz for middle elements.

### 4.2.2. Radiation Pattern Characteristics

The differential feeding array demonstrates improved radiation pattern properties compared to the pin-fed benchmark:

- **Gain:** The differential array achieves a maximum gain that is 1.25 dB higher than the pin-fed array.
- **Symmetry and Alignment:** The differential array maintains improved symmetry and exhibits a consistent  $0^\circ$  broadside alignment. In contrast, the pin-fed array distorts its pattern depending on the spacing, steering the main beam between  $-3^\circ$  and  $-15^\circ$  for  $0.6\lambda$  spacing, as shown in Figures 4.6(a) and 4.4(a).
- **Side Lobe Levels:** As shown in Table 4.1, side lobe levels remain relatively consistent across both arrays.
- **Cross Polarization:** The differential array exhibits slight improvements in cross-polarization, particularly during beam steering.
- **Beamwidth:** The  $-3$  dB beamwidth is approximately  $24^\circ$  for both arrays.

### 4.2.3. Phase Shift and Beam Steering

When phase shifts are applied:

- Both topologies exhibit similar beam-steering behavior, achieving comparable main beam angles after compensating for the initial misalignment in the pin-fed array at zero progressive phase shift.
- The differential array maintains pattern symmetry regardless of spacing, while the

pin-fed array experiences noticeable pattern distortion.

Array	Progressive phase shift (°)	Max Gain Angle (°)	L3X (dB)	L3Y (dB)	L3Y[45°](dB)	1st side lobe(dB/°)
Differential	0	0	13	-25	-25	-3/-42
	30	-9	13.62	-26	-26	-1.1/30
	60	-17	13.71	-14	-18	0.8/19
	90	-26	12.49	-14	-12	1/12
	120	-34	10.76	-30	-11	1/0
Pin fed	0	-2	10.6	-23	-26	-3/-41
	30	-11	11	-10	-13	-4.7/29
	60	-18	11	-12	-13	-0.2/19
	90	-26	10	-19	-14	0.6/11
	120	-35	8	-12	-14	-0.5/3

**Table 4.1:** Table comparing differential and pin fed linear array co-pol, x-pol, and sidelobe levels for  $0.5\lambda$  spacing between elements.

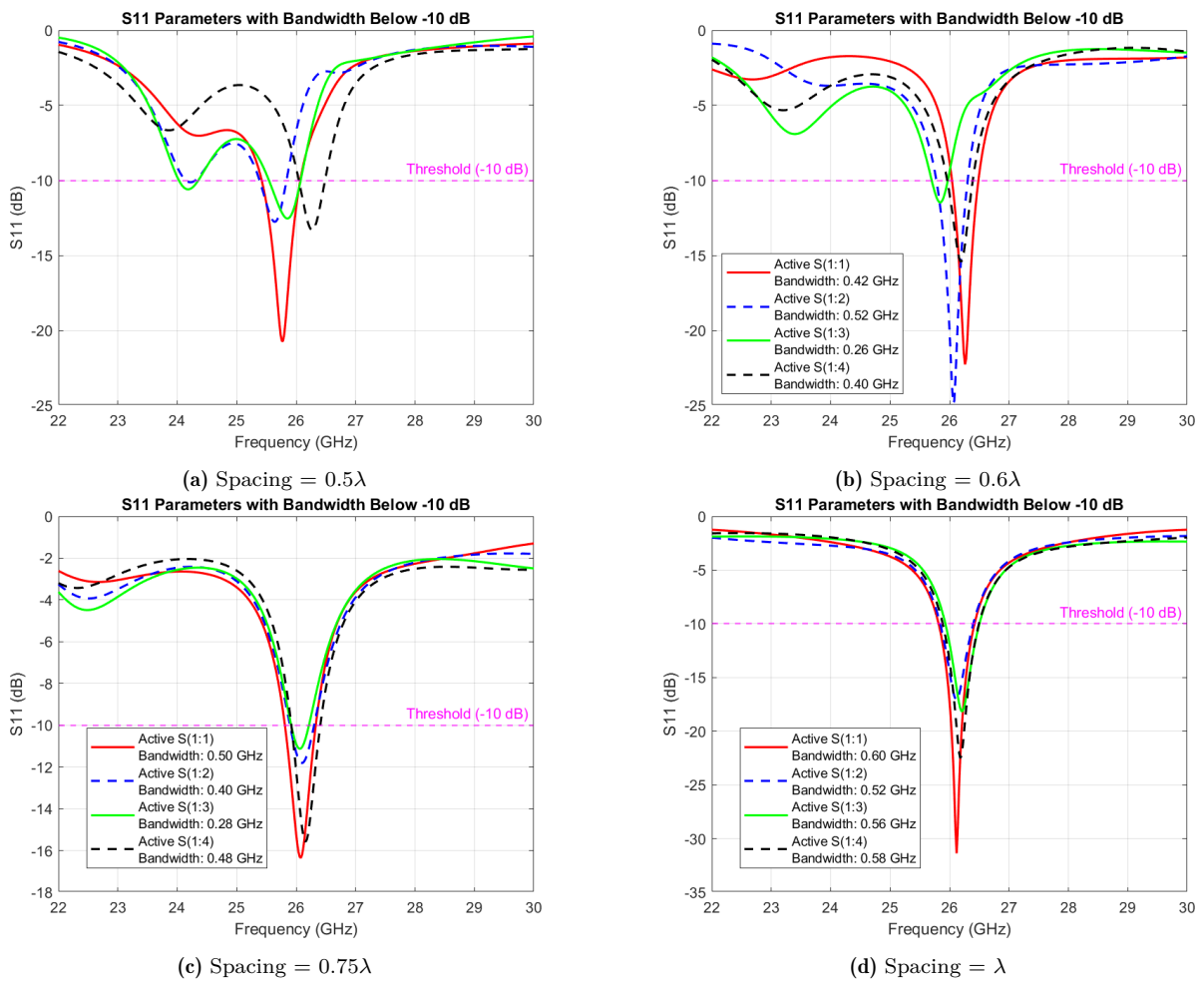


**Figure 4.2:** Four element pin fed array Active S-parameter at several spacings between elements. Progressive phase shift = 0.

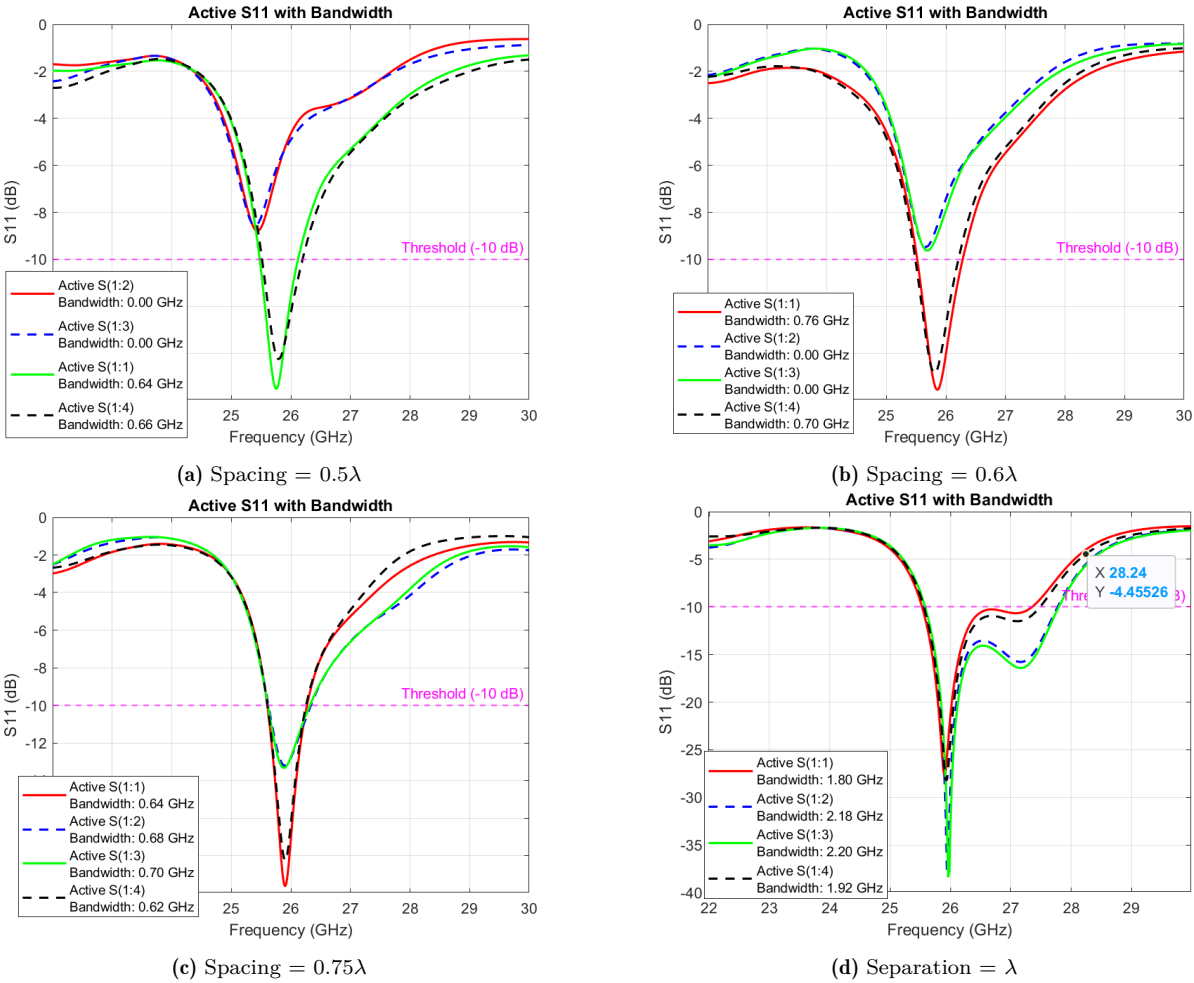
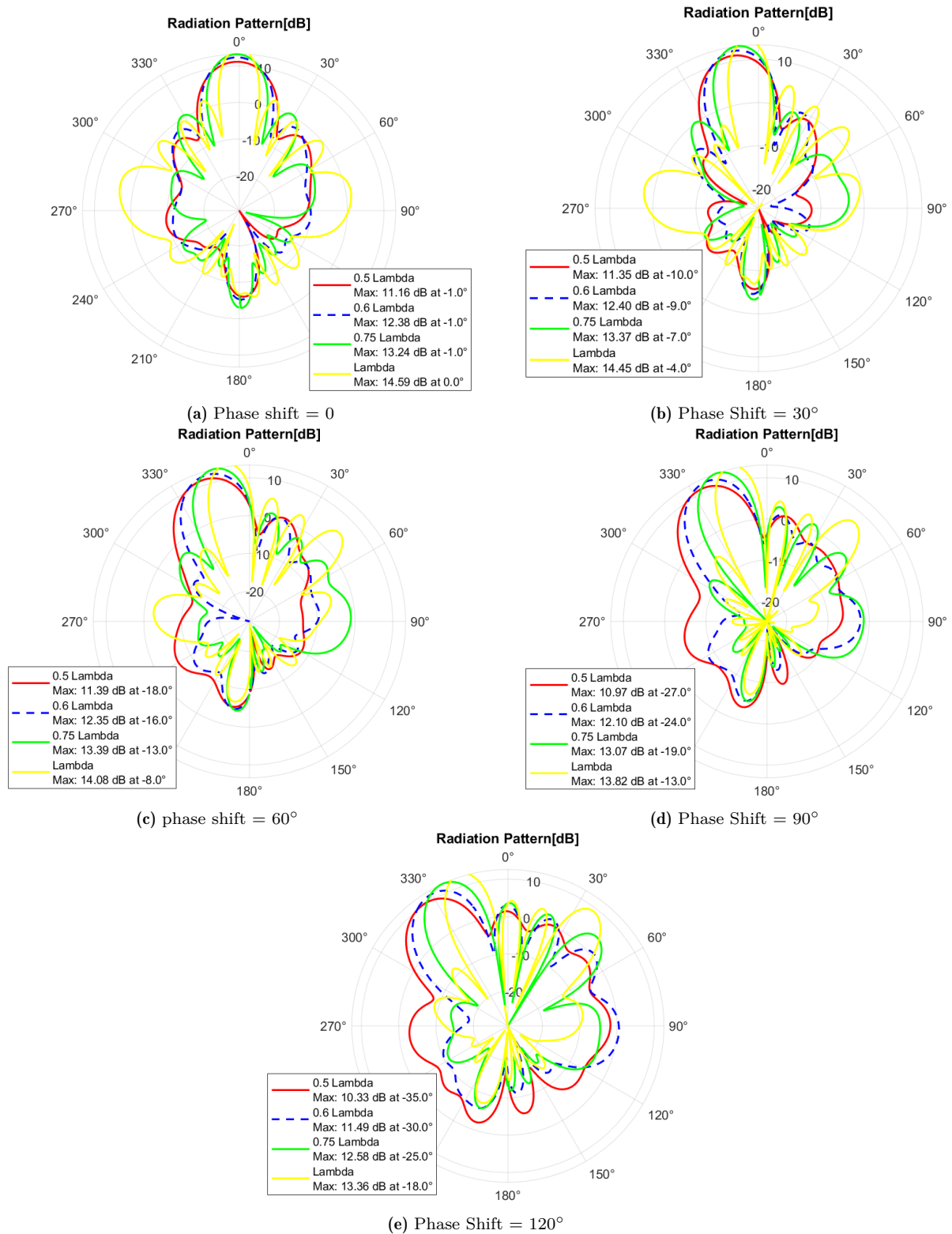


Figure 4.3: Four element differential array Active S-parameter at several spacings between elements. Progressive phase shift = 0.



**Figure 4.4:** Four element Differential array co-polarized realized gain results. 0°, 60°, 90°, 120° phase shifts are applied for several spacings between elements.

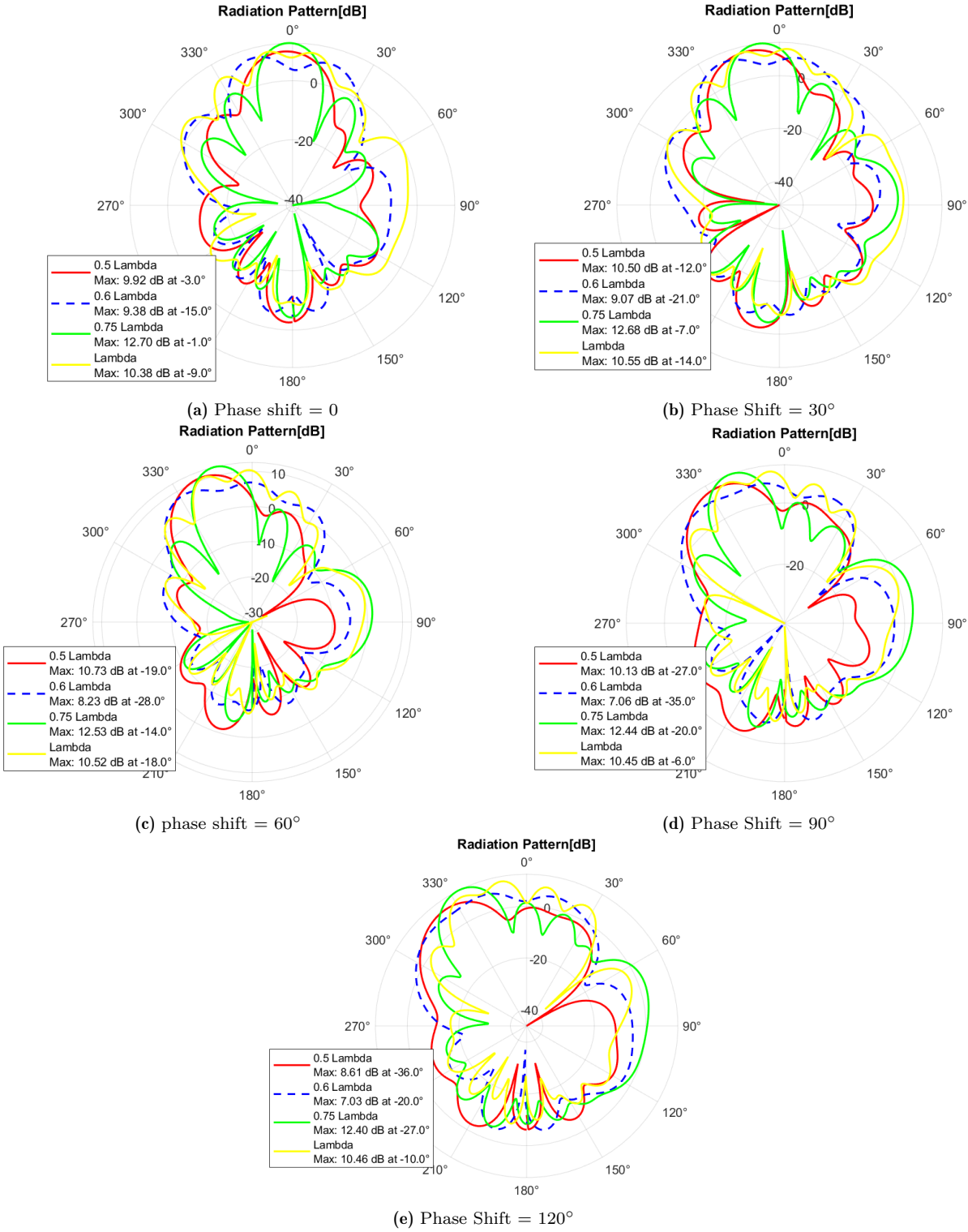
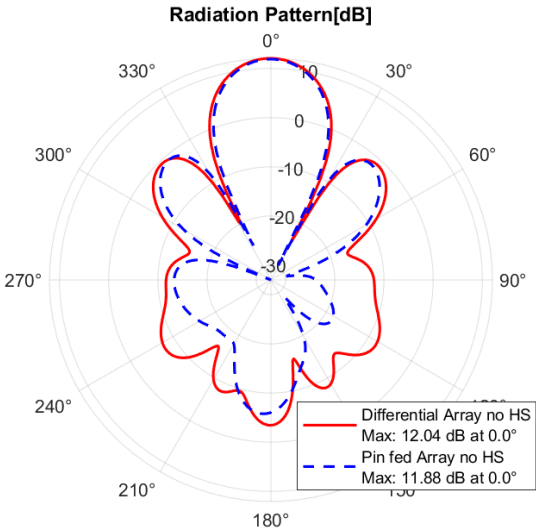
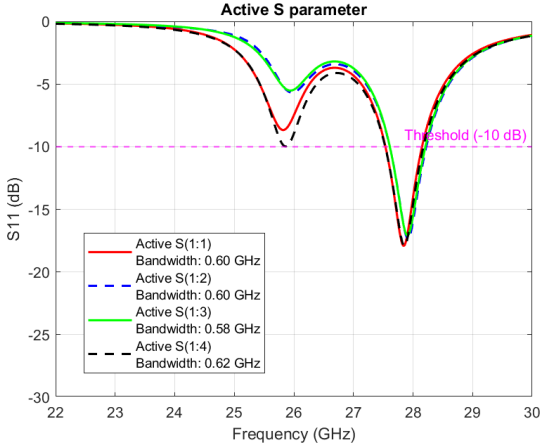


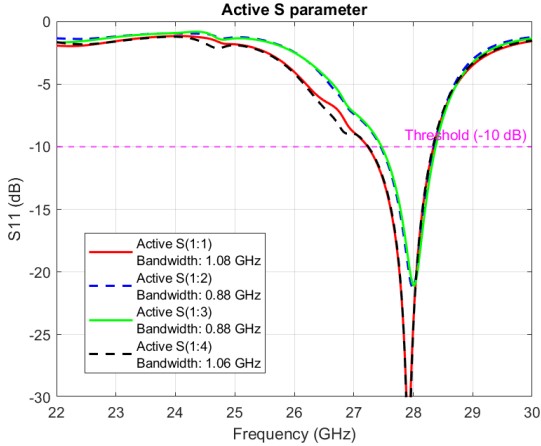
Figure 4.5: Four element Pin fed array co-polarized realized gain results. 0°, 60°, 90°, 120° phase shifts are applied for several spacings between elements.



(a) Co pol realized gain for differentially fed and pin fed array without heatsink at 28 GHz



(b) Active S parameter for pin fed array



(c) Active S parameter for differentially fed array

**Figure 4.6:** Realized gain and Active S parameter comparison of Pin fed and Differentially fed linear arrays. Gains are plotted for 28 GHz

# 5

## Conclusion

### 5.1. Conclusion

Recent research from MS3 on heatsink antennas offers a novel and cost-effective solution for antenna-in-package (AiP) heat management. The dual thermal and electromagnetic (EM) analysis illustrates the advantages of bonding a fin extrusion heatsink atop a shorted pin-fed patch antenna. However, several EM performance issues arise, notably a low impedance bandwidth attributed to the feeding technique. In addition, the presence of the heatsink affects the radiation pattern, creating asymmetry that can significantly impact the performance of communication, radar, or sensing applications. The implementation of the heatsink also exacerbates cross-polarization levels.

Taking this dual functional antenna as the benchmark, this thesis introduces an innovative approach to mitigate performance degradation in the impedance band and the radiation pattern of the patch caused by the heatsink. Firstly, the limited impedance bandwidth of the pin-fed shorted heatsink antenna is enhanced through aperture coupling feeding, resulting in a significant increase of 400 MHz compared to the benchmark. However, this improvement comes at the cost of notable distortion in the radiation pattern and a reduction in maximum gain. The maximum gain angle of the main beam was further deviated to  $-7^\circ$   $-11^\circ$ . Max gain was substantially reduced by 3 dB.

In addressing radiation pattern issues, a differential feeding scheme was introduced. A simple microstrip phase-shifted power divider (PSPD) was designed on the feeding side to ensure nearly equal amplitudes and a  $-180^\circ$  phase difference between the two ports. Furthermore, a reflector was introduced at  $\lambda/4$  to reduce the back radiation of the antenna. The results from the differentially fed patch element with heatsink reveal substantial improvements in radiation pattern symmetry, an increase in maximum gain of 1 dB, and enhanced impedance bandwidth of 100 MHz with the reflector, relative to the benchmark. The increase of the bandwidth is reduced compared to the differential fed shorted patch without heatsink. This is attributed to the effective elimination of resonances associated with the heatsink when applying differential feeding. Importantly, the radiation bandwidth of the differential patch remains consistent across the operational impedance bandwidth of the antenna, unlike the benchmark. The effects of amplitude and phase tapering in a single element was also explored, although the effectiveness was

found to be limited. Beamwidth control was achieved with the tapering of the phase and amplitude. Phase has a higher degree of impact than amplitude.

At the array level, the differential array showed increased coupling between elements when compared to pin fed array. For spacing less than or equal to  $0.6\lambda$ , the differential array the middle elements exhibit higher levels of coupling than the edge elements, not achieving the -10 dB threshold. For larger spacings, the differential array demonstrated widened active  $S_{11}$  bandwidth, achieving improvements up to approximately 1.8 GHz at  $\lambda$  spacing, while the pin fed array kept a relatively consistent impedance bandwidth at in all spacing. The radiation pattern of the differential array, like that of the element, exhibited high symmetry throughout its radiation bandwidth, consistently maintaining symmetry at  $0^\circ$  broadside, even as spacing varied. In contrast, the benchmark array experienced significant distortions. The maximum gain improved by 1.25 dB compared to the benchmark, and while cross-polarization levels were reduced, they equalized under progressive phase shifting. Both arrays maintained a  $-3dB$  beamwidth of  $24^\circ$ .

Both arrays exhibited comparable beam-steering performance when phase shifts were applied. However, the differential array retained symmetry regardless of spacing, whereas the pin-fed array demonstrated noticeable pattern distortions.

In summary, the differential feeding array presents a more robust design for applications requiring enhanced impedance bandwidth, gain, and consistent radiation pattern characteristics, particularly at larger spacings. Conversely, pin-fed arrays may still offer practical advantages in impedance performance across all elements at smaller spacings.

## 5.2. Recommendations

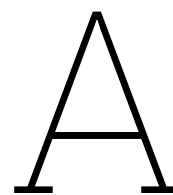
- A different feeding scheme could be explored to further enhance the results. Microstrip lines tend to be lossy and radiative, which negatively impacts the performance of the Pin-fed Shorted Patch Design (PSPD). Alternative transmission lines, such as striplines or substrate-integrated waveguides (SIW), may offer better suitability for this application.
- Differential feeding could have additional applications in inhomogeneous arrays, where asymmetric radiation patterns for edge elements are desirable. This approach can help achieve wide-angle beam steering, though with potential trade-offs in gain at the broadside.
- An extension to larger linear and planar arrays is essential. Coupled with this, improving the feeding scheme to provide circular polarization would further enhance the versatility of the system.
- Future work should consider incorporating mutual coupling reduction networks or frequency-selective surfaces (FSS) to mitigate the coupling between elements, which is exacerbated by the presence of heatsinks.
- Further thermal analysis at the array level is necessary. This would involve localizing hotspots, assessing heat generation, and studying the temperature rise to ensure optimal thermal management for larger and more complex systems.

# References

- [1] Wei Hong et al. “The Role of Millimeter-Wave Technologies in 5G/6G Wireless Communications”. In: *IEEE Journal of Microwaves* 1.1 (Jan. 2021), pp. 101–122. ISSN: 26928388. DOI: 10.1109/JMW.2020.3035541.
- [2] Yanki Aslan et al. “Thermal-aware synthesis of 5g base station antenna arrays: An overview and a sparsity-based approach”. In: *IEEE Access* 6 (2018), pp. 58868–58882. ISSN: 21693536. DOI: 10.1109/ACCESS.2018.2873977.
- [3] Abdullah Genc et al. *A Review of the EMI Effect on Natural Convection Heatsinks*. 2023. DOI: 10.1080/03772063.2021.1915188.
- [4] Muhammad Iqbal Rochman et al. “Impact of Device Thermal Performance on 5G mmWave Communication Systems”. In: Institute of Electrical and Electronics Engineers (IEEE), Nov. 2022, pp. 1–6. DOI: 10.1109/cqr54764.2022.9918612.
- [5] Chi Cong Nguyen et al. “Optimal Design of V-Shaped Fin Heat Sink for Active Antenna Unit of 5G Base Station”. In: *Journal of Engineering and Technological Sciences* 54.3 (May 2022). ISSN: 23385502. DOI: 10.5614/j.eng.technol.sci.2022.54.3.9.
- [6] Yanhua Guo et al. “Research on Heat Dissipation Performance and Long-term Reliability of the Flapping Wing Cooling Technology Applied to the 5G Communications Equipment”. In: *2021 27th International Workshop on Thermal Investigations of ICs and Systems, THERMINIC 2021*. Institute of Electrical and Electronics Engineers Inc., 2021. ISBN: 9781665418966. DOI: 10.1109/THERMINIC52472.2021.9626474.
- [7] Kevin P. Drummond et al. “A hierarchical manifold microchannel heat sink array for high-heat-flux two-phase cooling of electronics”. In: *International Journal of Heat and Mass Transfer* 117 (2018), pp. 319–330. ISSN: 00179310. DOI: 10.1016/j.ijheatmasstransfer.2017.10.015.
- [8] *Recent Advances in Space Technologies (RAST), 2015 7th International Conference on*. 2015. ISBN: 9781479976973.
- [9] Lance Covert and Jenshan Lin. “Simulation and measurement of a heatsink antenna: A dual-function structure”. In: *IEEE Transactions on Antennas and Propagation* 54.4 (Apr. 2006), pp. 1342–1345. ISSN: 0018926X. DOI: 10.1109/TAP.2006.872647.
- [10] Benjamin Rohrdantz et al. “Digital beamforming antenna array with polarisation multiplexing for mobile high-speed satellite terminals at Ka-band”. In: *The Journal of Engineering* 2016.6 (June 2016), pp. 180–188. ISSN: 2051-3305. DOI: 10.1049/joe.2015.0163.

- 
- [11] Bodhisatwa Sadhu, Xiaoxiong Gu, and Alberto Valdes-Garcia. “The More (Antennas), the Merrier: A Survey of Silicon-Based mm-Wave Phased Arrays Using Multi-IC Scaling”. In: *IEEE Microwave Magazine* 20.12 (Dec. 2019), pp. 32–50. ISSN: 15579581. DOI: 10.1109/MMM.2019.2941632.
- [12] Feza Turgay Celik and Yanki Aslan. *A Novel Heatsink Attached mm-Wave Active Patch Antenna With Adjustable Frequency and Cooling*. Tech. rep.
- [13] *2018 IEEE 20th Electronics Packaging Technology Conference (EPTC)*. IEEE, 2018. ISBN: 9781538676684.
- [14] David M Pozar. *A Review of Aperture Coupled Microstrip Antennas: History, Operation, Development, and Applications INTRODUCTION*. Tech. rep. 1996.
- [15] “Antenna Theory Analysis and Design Fourth Edition by Constantine A. Balanis”. In: ().
- [16] “Pozar\_Microwave Engineering(2012)”. In: ().
- [17] Lance Covert et al. *Dual-Function 3-D Heatsink Antenna for High-Density 3-D Integration*. Tech. rep.
- [18] Joaquin J. Casanova, Jason A. Taylor, and Jenshan Lin. “Design of a 3-D fractal heatsink antenna”. In: *IEEE Antennas and Wireless Propagation Letters* 9 (2010), pp. 1061–1064. ISSN: 15361225. DOI: 10.1109/LAWP.2010.2091104.
- [19] Abdullah Genc et al. “Heatsink Preselection Chart to Minimize Radiated Emission in Broadband on the PCB”. In: *IEEE Transactions on Electromagnetic Compatibility* 63.2 (Apr. 2021), pp. 419–426. ISSN: 1558187X. DOI: 10.1109/TEMC.2020.3019958.
- [20] Atef Alnukari et al. “Active heatsink antenna for radio-frequency transmitter”. In: *IEEE Transactions on Advanced Packaging* 33.1 (Feb. 2010), pp. 139–146. ISSN: 15213323. DOI: 10.1109/TADVP.2009.2023858.
- [21] Xuesong Zhang et al. “Fan-Out Antenna-in-Package Integration Using Heatsink Antenna”. In: *IEEE Transactions on Components, Packaging and Manufacturing Technology* 12.8 (Aug. 2022), pp. 1262–1270. ISSN: 21563985. DOI: 10.1109/TCPMT.2022.3195344.
- [22] Feza Turgay Celik, Alexander Yarovoy, and Yanki Aslan. “From Cooling to Coupling and Back: A Novel Beam-Switching Heatsink Antenna Array With CSRR Embedded Isolation Wall”. In: *IEEE Antennas and Wireless Propagation Letters* 22.11 (Nov. 2023), pp. 2690–2694. ISSN: 15485757. DOI: 10.1109/LAWP.2023.3302572.
- [23] Jiawei Qian et al. “Heatsink antenna array for millimeter-wave applications”. In: *IEEE Transactions on Antennas and Propagation* 68.11 (Nov. 2020), pp. 7664–7669. ISSN: 15582221. DOI: 10.1109/TAP.2020.2979194.
- [24] Yueping Zhang. “Differential Antennas: Fundamentals and Applications”. In: *Electromagnetic Science* 1.1 (Apr. 2023), pp. 1–17. ISSN: 2836-9440. DOI: 10.23919/emsci.2022.0002.

- [25] Yue Ping Zhang. “Design and experiment on differentially-driven microstrip antennas”. In: *IEEE Transactions on Antennas and Propagation* 55.10 (Oct. 2007), pp. 2701–2708. ISSN: 0018926X. DOI: 10.1109/TAP.2007.905832.
- [26] Neng Wu Liu et al. “A Low-Profile Aperture-Coupled Microstrip Antenna with Enhanced Bandwidth under Dual Resonance”. In: *IEEE Transactions on Antennas and Propagation* 65.3 (Mar. 2017), pp. 1055–1062. ISSN: 0018926X. DOI: 10.1109/TAP.2017.2657486.
- [27] Neng Wu Liu, Lei Zhu, and Wai Wa Choi. “A Differential-Fed Microstrip Patch Antenna with Bandwidth Enhancement under Operation of TM<sub>10</sub> and TM<sub>30</sub> Modes”. In: *IEEE Transactions on Antennas and Propagation* 65.4 (Apr. 2017), pp. 1607–1614. ISSN: 0018926X. DOI: 10.1109/TAP.2017.2670329.
- [28] Zijian Shao and Yue Ping Zhang. “Differential Shorted Patch Antennas”. In: *IEEE Transactions on Antennas and Propagation* 67.7 (July 2019), pp. 4438–4444. ISSN: 15582221. DOI: 10.1109/TAP.2019.2911394.
- [29] Lingzegang Wang et al. “A Miniaturized Differentially Fed Patch Antenna Based on Capacitive Slots”. In: *IEEE Antennas and Wireless Propagation Letters* 21.7 (July 2022), pp. 1472–1476. ISSN: 15485757. DOI: 10.1109/LAWP.2022.3171841.
- [30] Xujun Yang et al. “A differentially driven dual-polarized high-gain stacked patch antenna”. In: *IEEE Antennas and Wireless Propagation Letters* 17.7 (July 2018), pp. 1181–1185. ISSN: 15361225. DOI: 10.1109/LAWP.2018.2837116.
- [31] Xue Ying Wang et al. “Differential-Fed Dual-Polarized Dielectric Patch Antenna with Gain Enhancement Based on Higher Order Modes”. In: *IEEE Antennas and Wireless Propagation Letters* 19.3 (Mar. 2020), pp. 502–506. ISSN: 15485757. DOI: 10.1109/LAWP.2020.2964569.
- [32] Shaya Karimkashi et al. “Dual-polarization frequency scanning microstrip array antenna with low cross-polarization for weather measurements”. In: *IEEE Transactions on Antennas and Propagation* 61.11 (2013), pp. 5444–5452. ISSN: 0018926X. DOI: 10.1109/TAP.2013.2279996.
- [33] Tao Zhang et al. “A low-cost and high-gain 60-GHz differential phased array antenna in PCB process”. In: *IEEE Transactions on Components, Packaging and Manufacturing Technology* 8.7 (July 2018), pp. 1281–1291. ISSN: 21563950. DOI: 10.1109/TCPMT.2018.2839342.
- [34] Duixian Liu et al. “Packages with integrated 60-GHz aperture-coupled patch antennas”. In: *IEEE Transactions on Antennas and Propagation* 59.10 (Oct. 2011), pp. 3607–3616. ISSN: 0018926X. DOI: 10.1109/TAP.2011.2163760.
- [35] Yingqi Zhang et al. “Broadband Dual-Polarized Differential-Fed Filtering Antenna Array for 5G Millimeter-Wave Applications”. In: *IEEE Transactions on Antennas and Propagation* 70.3 (Mar. 2022), pp. 1989–1998. ISSN: 15582221. DOI: 10.1109/TAP.2021.3118800.
- [36] Zijian Shao and Yue Ping Zhang. “Miniaturization of Differentially-Driven Microstrip Planar Inverted F Antenna”. In: *IEEE Transactions on Antennas and Propagation* 67.2 (Feb. 2019), pp. 1280–1283. ISSN: 0018926X. DOI: 10.1109/TAP.2018.2883575.



# Appendix A

Ratio	Alpha(deg)	Bandwidth(GHz) S(1:1)	Bandwidth(GHz) S(2:1)	Max Gain(dB)	Max Gain Angle (w.r.t theta=0,deg)	Gain[dB] @-30deg	Gain[dB] @-45deg	Gain[dB] @-60deg
1	90	0.4151	1.1028	3.51	-6	-0.4313	-7.44	-9.88
1	105	0.6031	1.2249	4.175	-5	0.54	-6.64	-13.43
1	120	1.1704	0.75	5.1983	-3	1.2694	-5.68	-19.1
1	135	1.024	0.7744	5.7416	-2	1.8375	-4.75	-36.38
1	150	0.8763	0.7657	6.1165	-1	2.28	-3.9	-22.05
1	165	0.7806	0.7474	6.3378	-1	2.62	-3.15	-15.5
1	180	0.7404	0.7437	6.411	0	2.89	-2.488	-11.93
1	195	0.7475	0.7809	6.3384	1	3.08	-1.9	-9.46
1	210	0.7654	0.8774	6.1179	1	3.2	-1.38	-7.57
1	225	0.7735	1.0256	5.7436	2	3.26	-0.93	-6.03
1	240	0.7481	1.1717	5.2011	3	3.23	-0.54	-4.774
1	255	0.6554	1.2249	4.4698	4	3.12	-0.22	-3.64
1	270	0.407	1.101	3.515	6	2.89	0.03	-2.69
0.9	90	0.3832	1.1519	3.5049	5	-0.25	-6.95	-9.87
0.9	105	0.6394	1.2702	4.46	4	0.65	-6.26	-13.4
0.9	120	0.7385	1.1978	5.1937	3	1.36	-5.4	-18.98
0.9	135	0.7717	1.0245	5.738	2	1.91	-4.53	-32.41
0.9	150	0.772	0.855	6.11	1	2.34	-3.73	-21.82
0.9	165	0.7627	0.7503	6.33	1	2.68	-3.01	-15.48
0.9	180	0.7659	0.7161	6.4078	0	2.94	-2.36	-11.91
0.9	195	0.8043	0.7284	6.3364	-1	3.13	-1.8	-9.45
0.9	210	0.8925	0.7567	6.1168	-2	3.25	-1.29	-7.56
0.9	225	1.0216	0.7749	5.7426	-3	3.31	-0.84	-6.03
0.9	240	1.1444	0.7589	5.202	-3	3.3	-0.45	-4.74
0.9	255	1.1815	0.6749	4.4747	-5	3.18	-0.13	-3.64
0.9	270	1.085	0.4396	3.5317	-6	2.96	0.11	-2.69
0.8	90	0.3578	1.1519	3.5049	5	-0.08	-6.44	-9.82
0.8	105	0.6119	1.2702	4.46	4	0.78	-5.86	-13.29
0.8	120	0.7277	1.1978	5.1937	3	1.46	-5.09	-18.57
0.8	135	0.7683	1.0181	5.738	2	1.99	-4.3	-27.44
0.8	150	0.7769	0.821	6.1138	1	2.41	-3.54	-21.12
0.8	165	0.7758	0.7066	6.3341	1	2.74	-2.86	-15.32
0.8	180	0.7854	0.6776	6.4082	0	2.99	-2.24	-11.86
0.8	195	0.8248	0.72	6.3364	-1	3.19	-1.69	-9.42
0.8	210	0.9046	0.7435	6.11	-2	3.3	-1.19	-7.55
0.8	225	1.0157	0.7738	5.7426	-3	3.37	-0.75	-6.03
0.8	240	1.1153	0.7681	5.202	-3	3.35	-0.37	-4.74
0.8	255	1.1353	0.6932	4.4747	-5	3.25	-0.04	-3.64
0.8	270	1	0.4681	3.5317	-6	3.03	0.2	-2.7
0.7	90	0.3303	1.2812	3.4719	4	0.12	-5.9	-9.74
0.7	105	0.6026	1.3864	4.4277	3	0.93	-5.42	-13.07
0.7	120	0.7147	1.2596	5.1609	2	1.57	-4.75	-17.85
0.7	135	0.763	1	5.7046	2	2.08	-4.04	-23.71
0.7	150	0.7797	0.7673	6.0816	1	2.49	-3.34	-19.99
0.7	165	0.7864	0.6408	6.3038	0	2.81	-2.69	-15.02
0.7	180	0.8017	0.6215	6.3784	0	3.06	-2.1	-11.74
0.7	195	0.8409	0.6644	6.3095	-1	3.24	-1.56	-9.37
0.7	210	0.9125	0.7241	6.0952	-2	3.36	-1.08	-7.52
0.7	225	1	0.77	5.7284	-3	3.42	-0.65	-6.02
0.7	240	1.08	0.7775	5.198	-4	3.41	-0.27	-4.75
0.7	255	1.08	0.7142	4.4863	-5	3.31	0.04	-3.66
0.7	270	0.9474	0.5019	3.569	-7	3.11	0.29	-2.71
0.6	90	0.3007	1.3647	3.4054	4	0.35	-5.34	-9.6
0.6	105	0.5812	1.4627	4.403	3	1.09	-4.96	-12.73
0.6	120	0.6994	1.2961	5.132	2	1.69	-4.39	-16.85
0.6	135	0.7551	0.9672	5.6731	1	2.18	-3.75	-20.74
0.6	150	0.7798	0.6765	6.0471	0	2.57	-3.11	-18.55
0.6	165	0.7942	0.5332	6.2694	0	2.88	-2.5	-14.55
0.6	180	0.8142	0.5336	6.3455	-1	3.12	-1.94	-11.54
0.6	195	0.8528	0.6077	6.2781	-2	3.3	-1.43	-9.28
0.6	210	0.9151	0.6945	6.0669	-2	3.42	-0.96	-7.48
0.6	225	0.9902	0.7619	5.7061	-3	3.48	-0.54	-6
0.6	240	1.046	0.787	5.1844	-4	3.47	-0.17	-4.75
0.6	255	1.0323	0.7388	4.4862	-5	3.38	0.14	-3.67
0.6	270	0.888	0.5428	3.5908	-7	3.19	0.38	-2.74
0.5	90	0.2866	1.4649	3.437	3	0.6	-4.74	-9.39
0.5	105	0.5569	1.5568	4.3701	2	1.27	-4.45	-12.23
0.5	120	0.6808	1.3363	5.0883	1	1.83	-3.98	-15.62
0.5	135	0.7438	0.8924	5.6238	1	2.29	-3.42	-18.2
0.5	150	0.7765	0.4968	5.9951	0	2.66	-2.85	-16.93
0.5	165	0.7977	0.3124	6.2145	-1	2.95	-2.29	-13.9
0.5	180	0.8219	0.3725	6.2913	-1	3.84	-1.77	-11.24
0.5	195	0.8588	0.515	6.2276	-2	3.36	-1.28	-9.13
0.5	210	0.9112	0.6473	6.0213	-3	3.48	-0.84	-7.41
0.5	225	0.9687	0.7461	5.6681	-4	3.53	-0.43	-5.98
0.5	240	1	0.7953	5.1591	-5	3.53	-0.08	-4.75
0.5	255	0.9738	0.7678	4.408	-6	3.45	0.23	-3.7
0.5	270	0.8258	0.5941	3.6143	-8	3.27	0.47	-2.79

# B

## Appendix B

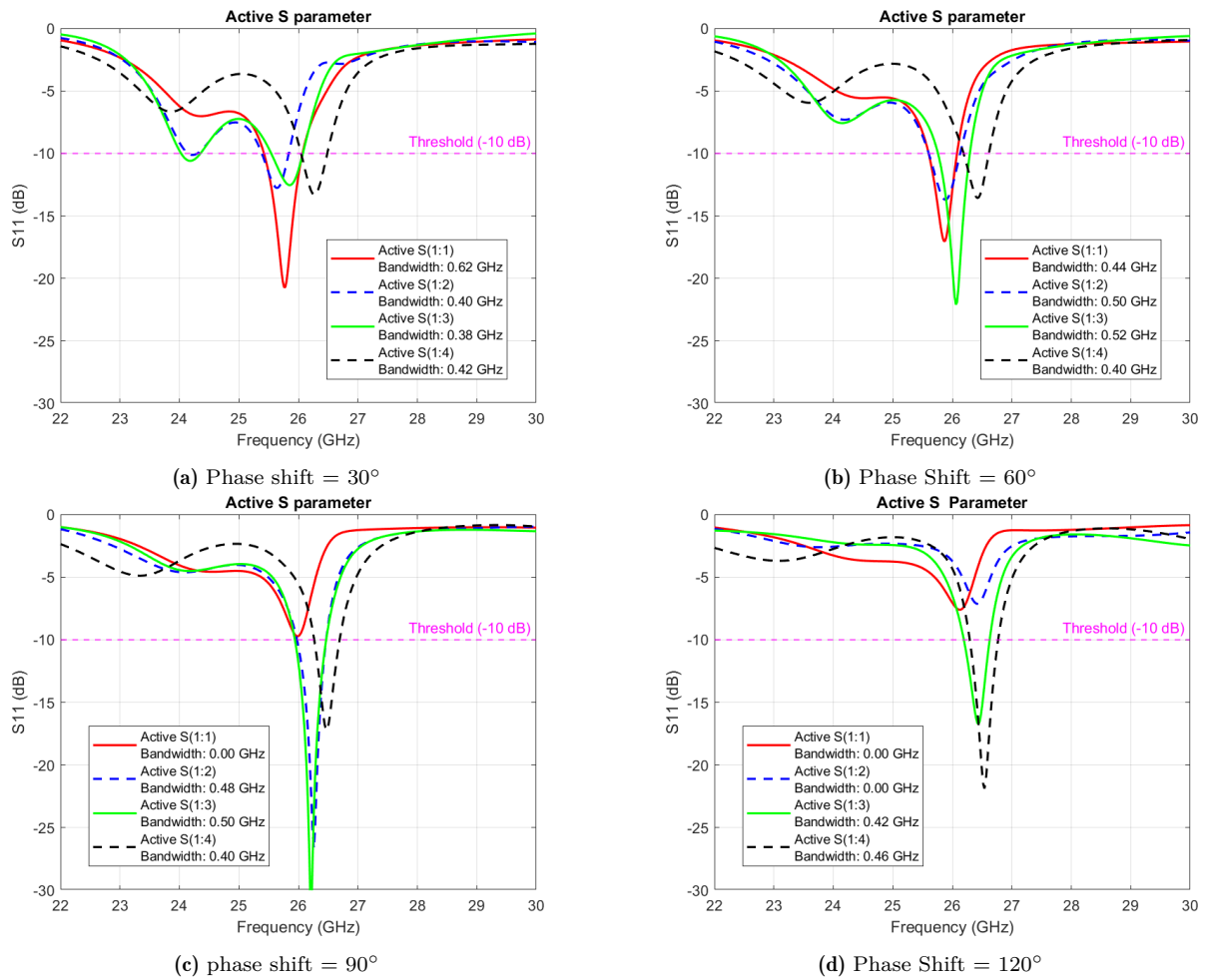


**Figure B.1:** Four element pin fed array with heatsink active S parameters with a progressive phase shift of:  $30^\circ$ ,  $60^\circ$ ,  $90^\circ$ ,  $120^\circ$

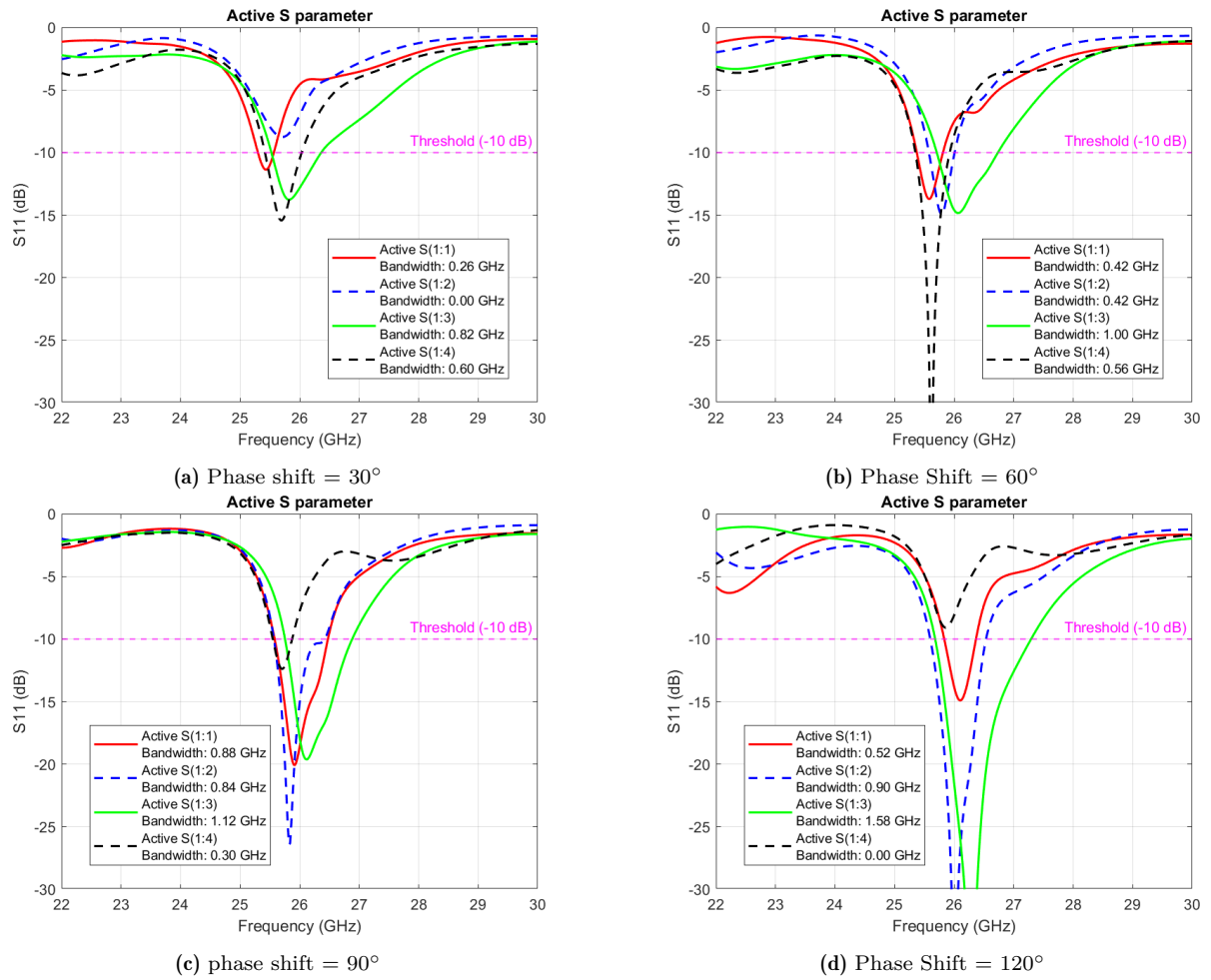


**Figure B.2:** Four element differentially fed array with heatsink active S parameters with a progressive phase shift of:  $30^\circ$ ,  $60^\circ$ ,  $90^\circ$ ,  $120^\circ$